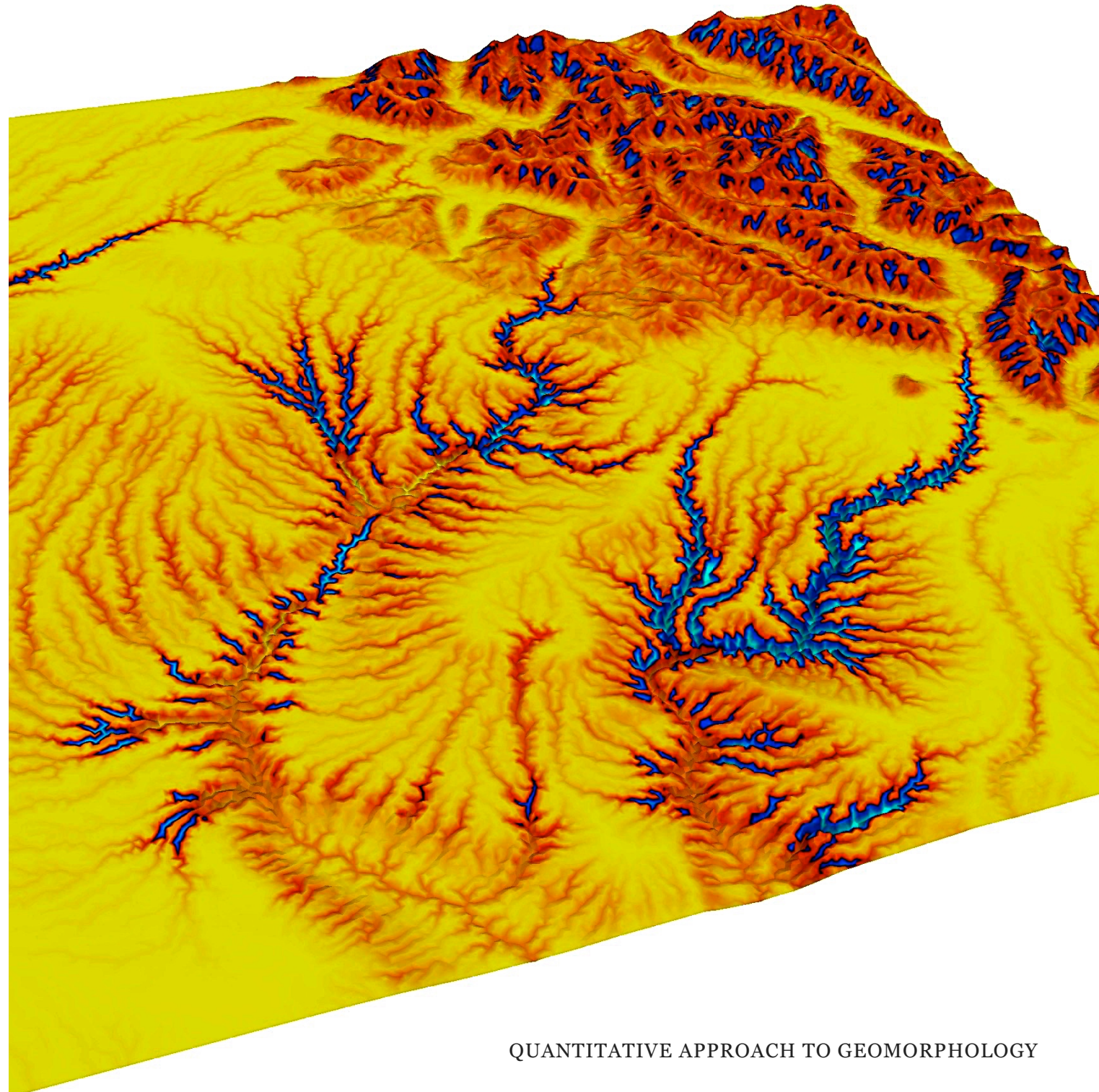


Tectonic Geomorphology



Geomorphology in a nutshell



SECTION 1

River landforms

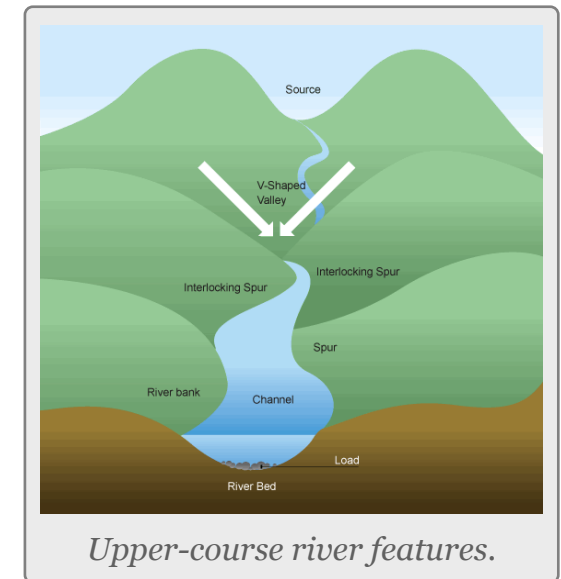
KEY POINTS

1. Differences in the characteristics of a stream from source to sink.
2. Definition of drainage basin terms.
3. Characterization of fluvial network.

Most rivers are considered as reaches with different geomorphological characteristics. The most simple division generally made is to divide the river into **Upper**, **Middle** and **Lower River** reaches.

UPPER RIVER

The uppermost portion of a river system includes the river headwaters and low-order streams at higher elevation. The upper river basin is usually characterized by steep gradients and by erosion that carries sediment downstream. Streams in this upper region are usually steep and torrential, and often include rapids and waterfalls. These streams generally have little floodplain, although part of the bank and surrounding land may be wetted during periods of high flow.



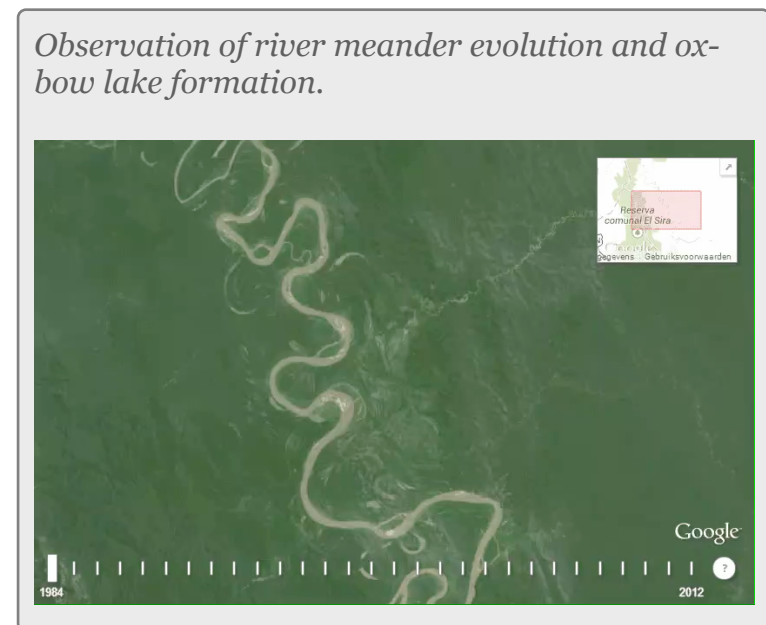
Upper-course river features.

MIDDLE RIVER

In the middle course the river has more energy and a high volume of water. The gradient here is gentle and lateral erosion has widened the river channel. The river channel has also deepened. A larger river channel means there is less friction, so the water flows faster:

- As the river erodes laterally, to the right side then the left side, it forms large bends, and then horseshoe-like loops called meanders.
- The formation of meanders is due to both deposition and erosion and meanders gradually migrate downstream.

- The force of the water erodes and undercutts the river bank on the outside of the bend where water flow has most energy due to decreased friction.
- On the inside of the bend, where the river flow is slower, material is deposited, as there is more friction.
- Over time the horseshoe become tighter, until the ends become very close together. As the river breaks through, e.g. during a flood when the river has a higher discharge and more energy, and the ends join, the loop is cut-off from the main channel. The cut-off loop is called an oxbow lake.



LOWER RIVER

In the lower course, the river has a high volume and a large discharge. The river channel is now deep and wide and the landscape around it is flat. However, as a river reaches the end of its journey, energy levels are low and deposition takes place.

FLOODPLAINS

The river now has a wide floodplain. A floodplain is the area around a river that is covered in times of flood. A floodplain is a very fertile area due to the rich alluvium deposited by floodwaters. This makes floodplains a good place for agriculture. A build up of alluvium on the banks of a river can create levees, which raise the river bank.

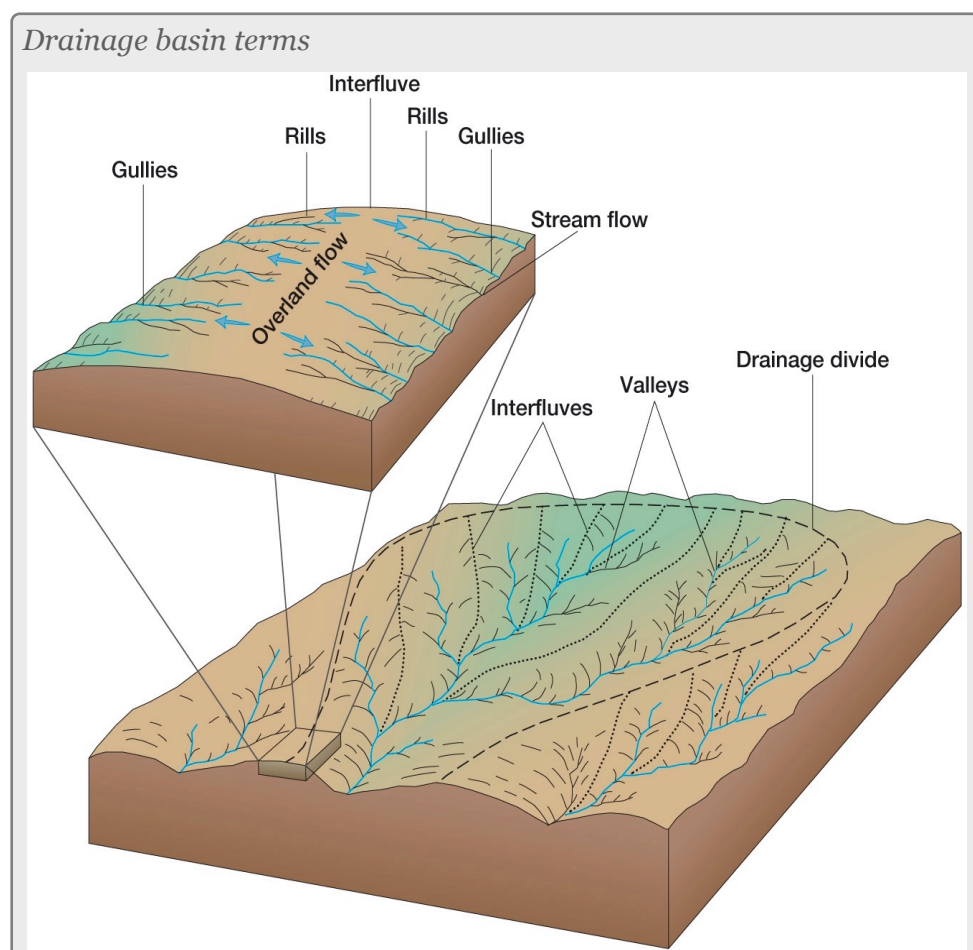
DELTAS

TYPE OF DELTA	EXAMPLE
Arcuate or fan-shaped - the land around the river mouth arches out into the sea and the river splits many times on the way to the sea, creating a fan effect.	<p>Niger Delta</p>
Cuspate - the land around the mouth of the river juts out arrow-like into the sea.	<p>Ebro Delta</p>
Bird's foot - the river splits on the way to the sea, each part of the river juts out into the sea, rather like a bird's foot.	<p>Mississippi Delta</p>

Deltas are found at the mouth of large rivers - for example, the Mississippi. A delta is formed when the river deposits its material faster than the sea can remove it.

DRAINAGE BASIN DEFINITIONS

The drainage basin is the land surface drained by a stream system; an interflue is a divide, an area of higher land that separates one valley from the next (within a drainage basin); a drainage divide is an interflue that separates two drainage basins. The drainage pattern of the river reflects the rock materials and landscape through which the river flows; stream order is a hierarchical system to define river system complexity; and base level is a level below which a river cannot erode its channel.



STREAM ORGANIZATION

Seen from above, river systems display a tree-like pattern, with many small streams feeding into fewer larger rivers and eventually into one very large river.



Schematic diagram of Strahler stream order.

Many systems have been developed to classify the different “levels” of streams in this pattern. In the system devised by **Strahler**, each level of stream is assigned an order. Order 1 streams are the very smallest, uppermost streams (i.e., with no upstream tributaries). Two order 1 streams combine to form a stream of order 2. Order 3 streams are formed from the confluence of two order 2 streams. Each higher order of stream is formed from the confluence of two lower order streams, and the watersheds of lower-order streams are included within the watersheds of higher order streams. Orders 10–12 correspond to the main channels of large world rivers. In general, individual streams get wider and longer with increasing stream order.

Characteristics of a river system depend on the landscape, climate, other geographical features and natural processes. Most river systems can be divided into different sections from the headwaters to the river mouth.

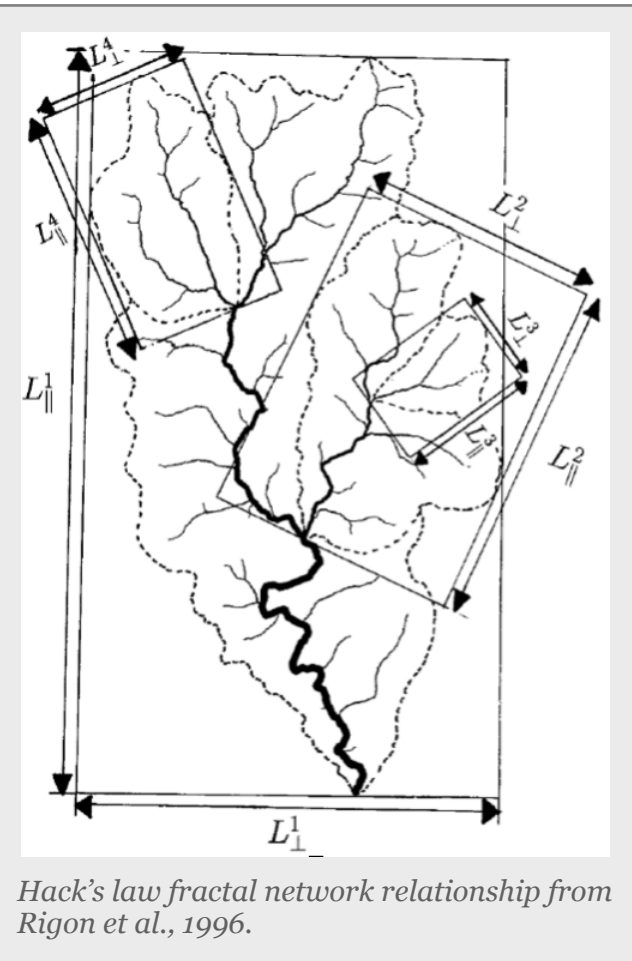
HIERARCHICAL ORGANIZATION OF FLUVIAL NETWORK

The physical characteristics of river systems are organized in a nested hierarchy, with physical processes operating at larger scales influencing those at successively finer resolutions, ultimately controlling the

micro-scale distribution of hydraulic and sediment transport processes. The micro-, meso- and reach scales are therefore all equally critical elements within this hierarchy, with different geomorphic and ecological processes being relevant at each resolution.

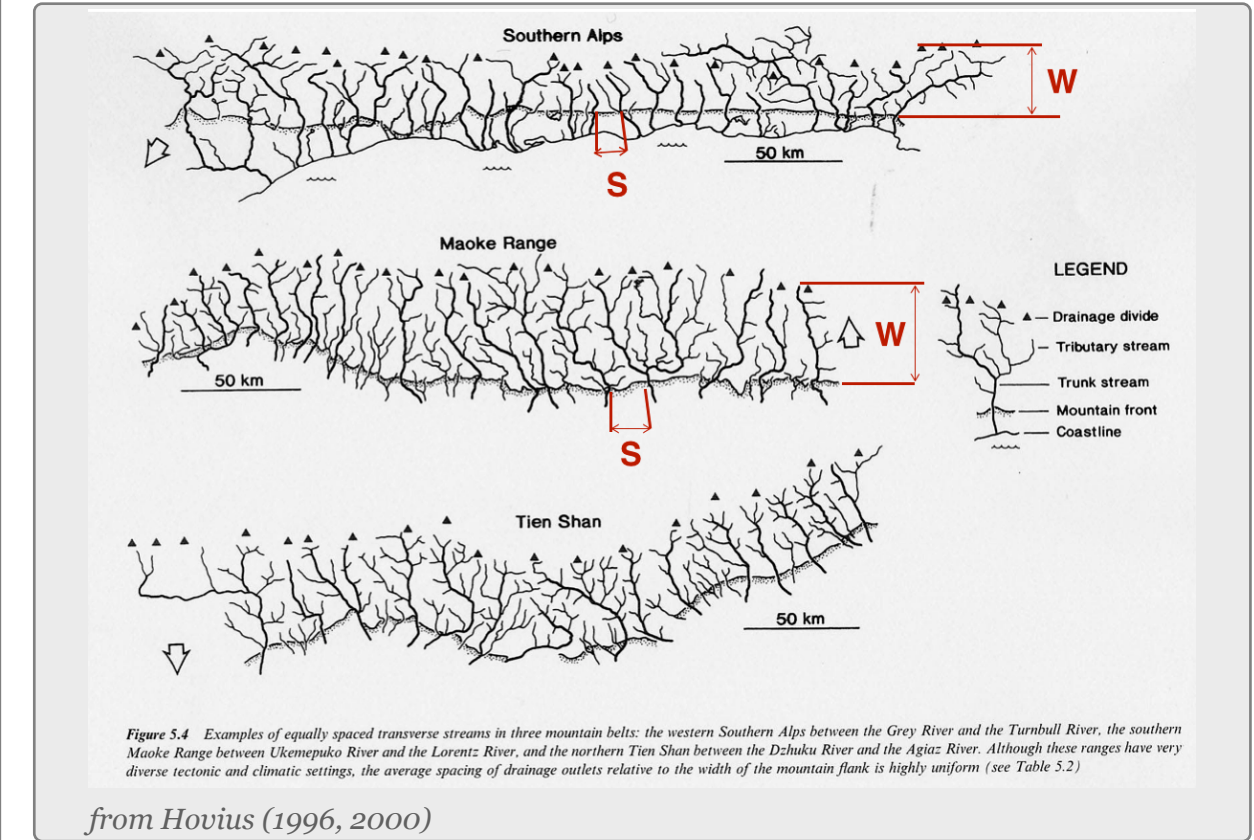
Defining S as the average spacing of outlets for major drainages and W the half-width of major mountain ranges, Hovius (1996) managed to fit a regression curve that yields to:

$$S = 0.46 \times W + 0.798$$



Large-scale observations have allowed thorough comparisons across scales defining fractal river basins [Mandelbrot, 1977, 1983]. One outstanding example of fractal relation is Hack's law [Hack, 1957; Mandelbrot, 1983; Rigon et al., 1996] relating the upstream length L_i at a given position i to the total cumulative area A_i at that position, seen quite early as a signature of fractal geometry. With β a constant between 1.4 and 1.7 and α comprised between 0.5 and 0.6 for natural rivers, Hack's law scales to:

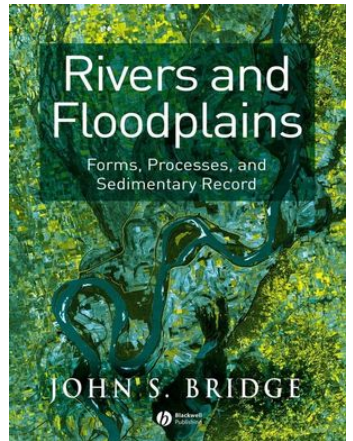
$$L_i = \beta A_i^\alpha$$



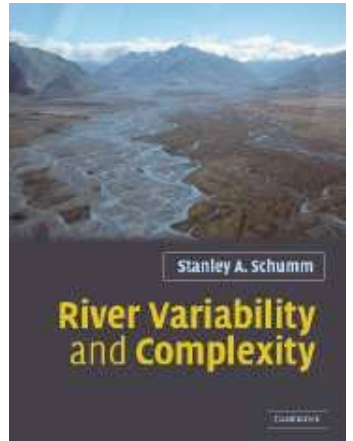
REFERENCES

- Hack, J. T. (1957), Studies of longitudinal profiles in Virginia and Maryland, U.S. Geol. Surv. Prof. Pap., 294-B, 52 pp.
- Hovius, N. (1996), Regular spacing of drainage outlets from linear mountain belts, Basin Res., 8, 29–44.
- Hovius, N., C. P. Stark, and P. A. Allen (1997), Sediment flux from a mountain belt derived by landslide mapping, Geology, 25, 231–234.
- Mandelbrot, B. B. (1977), Fractals: Form, Chance and Dimension, W. H. Freeman, New York.
- Mandelbrot, B. B. (1983), The Fractal Geometry of Nature, W. H. Freeman, New York.
- Rigon, R., I. Rodriguez-Iturbe, A. Maritan, A. Giacometti, D. G. Tarboton, and A. Rinaldo (1996), On Hack's law, Water Resour. Res., 32, 3367–3374.

FURTHER READING



Bridge, J. S. 2003. Rivers and floodplains: forms, processes, and sedimentary record. Oxford, UK: Blackwell Pub.



Schumm, Stanley A.. River Variability and Complexity. 1st ed. Cambridge: Cambridge University Press, 2005. Cambridge Books Online. Web. 26 February 2015.

SECTION 2

Sediment transport concept

KEY POINTS

1. Sediment transport by stream.
2. Modes of transport.
3. Sediment entrainment.

SOME DEFINITIONS

Sediment transport is critical to understanding how rivers work because it is the set of processes that mediates between the flowing water and the channel boundary. Erosion involves the removal and transport of sediment (mainly from the boundary) and deposition involves the transport and placement of sediment on the boundary. Erosion and deposition are what form the channel of any alluvial river as well as the floodplain through which it moves.

The amount and size of sediment moving through a river channel are determined by three fundamental controls: *competence*, *capacity* and *sediment supply*.

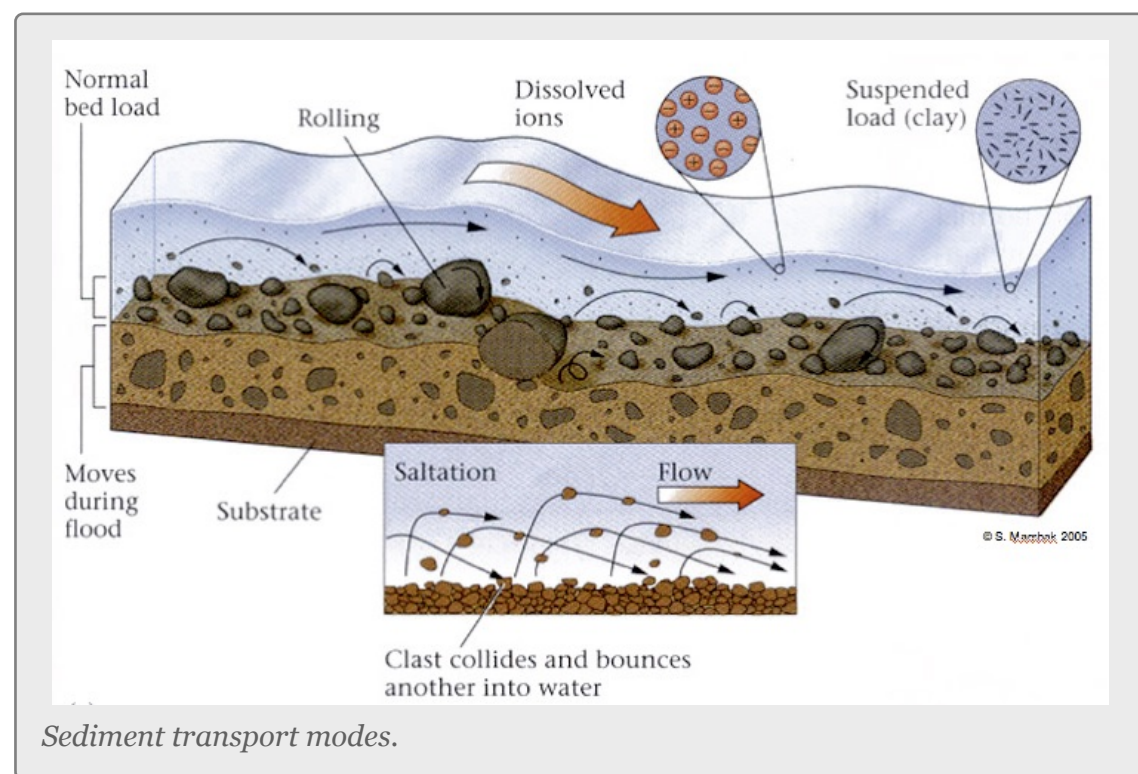
Competence refers to the largest size (diameter) of sediment particle or grain that the flow is capable of moving; it is a hydraulic limitation. If a river is sluggish and moving very slowly it simply may not have the power to mobilize and transport sediment of a given size even though such sediment is available to transport. So a river may be competent or incompetent with respect to a given grain size. If it is incompetent it will not transport sediment of the given size. If it is competent it may transport sediment of that size if such sediment is available (that is, the river is not supply-limited).

Capacity refers to the maximum amount of sediment of a given size that a stream can transport in traction as bedload. Given a supply of sediment, capacity depends on channel gradient, discharge and the calibre of the load (the presence of fines may increase fluid density and increase capacity; the presence of large particles may obstruct the flow and reduce capacity). Capacity transport is the competence-limited sediment transport (mass per unit time) predicted by all sediment-transport equations, examples of which we will examine below. Capacity transport only occurs when sediment supply is abundant (non-limiting).

Sediment supply refers to the amount and size of sediment available for sediment transport. Capacity transport for a given grain size is only achieved if the supply of that calibre of sediment is not limiting (that is, the maximum amount of sediment a stream is capable of transporting is actually available). Because of these two different potential constraints (hydraulics and sediment supply) distinction is often made between supply-limited and capacity-limited transport. Most rivers probably function in a sediment-supply limited condition although we often assume that this is not the case.

Much of the material supplied to a stream is so fine (silt and clay) that, provided it can be carried in suspension, almost any flow will transport it. Although there must be an upper limit to the capacity of the stream to transport such fines, it is probably never reached in natural channels and the amount moved is limited by supply. In contrast, transport of coarser material (say, coarser than fine sand) is largely capacity limited.

MODES OF SEDIMENT TRANSPORT



The sediment load of a river is transported in various ways although these distinctions are to some extent arbitrary and not always very practical in the sense that not all of the components can be separated in practice:

- I. Dissolved load
- II. Suspended load
- III. Intermittent suspension (saltation) load
- IV. Wash load
- V. Bed load

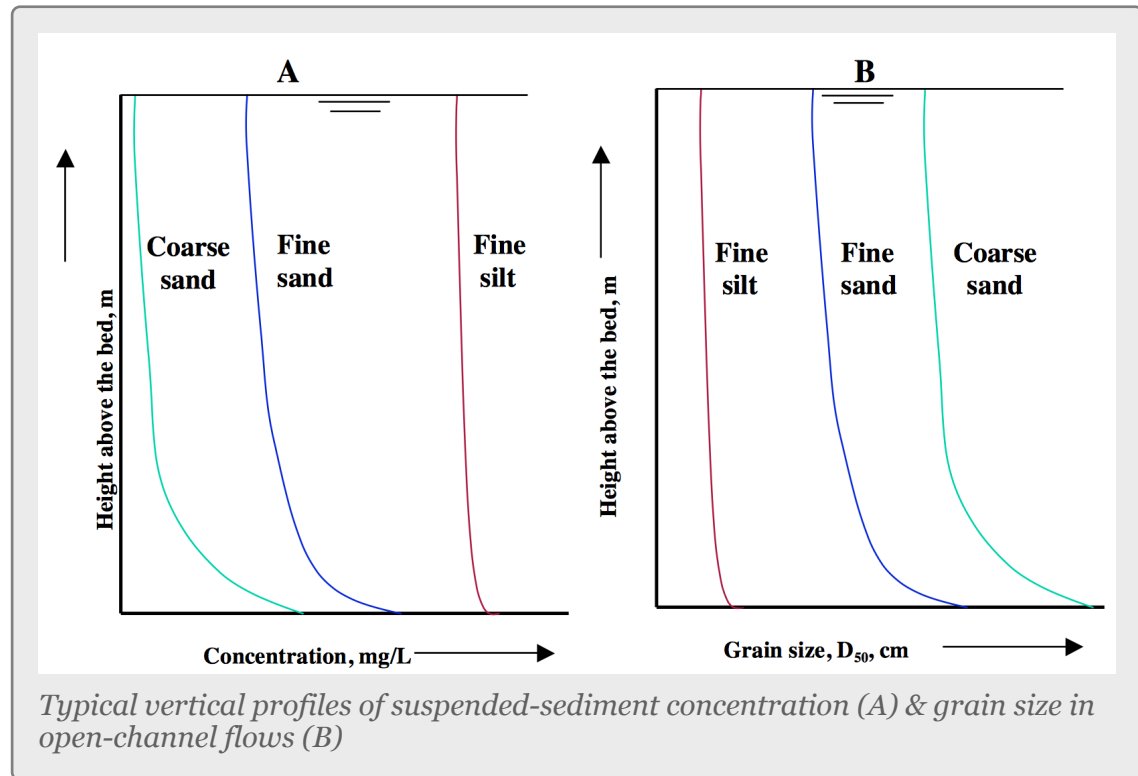
Dissolved load is material that has gone into solution and is part of the fluid moving through the channel. Since it is dissolved, it does not depend on forces in the flow to keep it in the water column.

In sediment-transport theory an important distinction is made between dissolved material and clastic material. Clastic material is all the particulate matter (undissolved material) carried by a river regardless of the grain size. The clastic load of a river is moved by several mechanisms that are the basis for recognizing the two principal sediment-transport modes: *suspended-sediment load* and *bed-material load*.

Suspended-sediment load is the clastic (particulate) material that moves through the channel in the water column. These materials, mainly silt and sand, are kept in suspension by the upward flux of turbulence generated at the bed of the channel. The upward currents must equal or exceed the particle fall-velocity for suspended-sediment load to be sustained.

The size and concentration of suspended-sediment typically varies logarithmically with height above the bed. That is, concentration and grain size form linear plots with the logarithm of height above the bed. Coarse sand is highly concentrated near the bed and declines with height at a faster rate than does fine sand. Fine silt is so easily suspended that it is far more uniformly distributed in a vertical section

than is the coarser material. Similarly, the grain-size distribution within a sample of sand displays far more vertical variation than does the vertical distribution of grain size within the silt range. The former is too large for the flow to move much of it into the upper water column and the latter is so small and easily suspended that it is well represented at all levels thus giving rise to a more uniform grain-size profile.



Although **wash load** is part of the suspended-sediment load it is useful here to make a distinction. Unlike most suspended-sediment load, wash load does not rely on the force of mechanical turbulence generated by flowing water to keep it in suspension. It is so fine (in the clay range) that it is kept in suspension by thermal molecular agitation (sometimes known as Brownian motion, named for the early 19th-century botanist who described the random motion of microscopic pollen spores and dust). Because these clays are always in suspension, wash load is that component of the particulate or clastic load that is “washed” through the river system. Unlike coarser suspended-sediment, wash load tends to be uniformly distributed throughout the

water column. That is, unlike the coarser load, it does not vary with height above the bed.

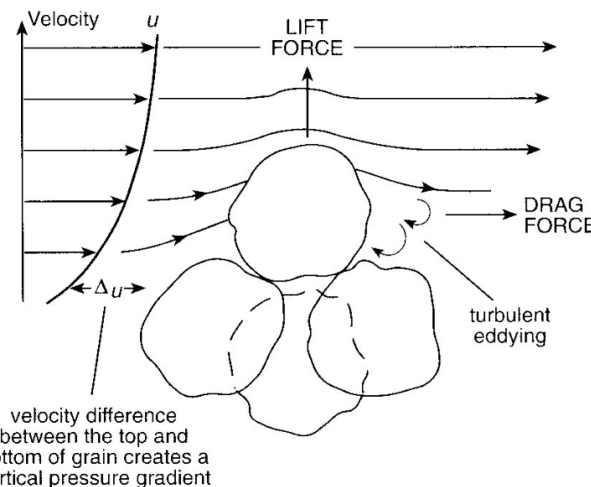
Distinction is made between fully-suspended load and bed load by classifying the intermediate and transient transport state as **saltation load** transport. These are particles that bounce along the channel, partly supported by the turbulence in the flow and partly by the bed. They follow a distinctively asymmetric trajectory. Saltation load may be measured as suspended load (when in the water column) or as bed-load (when on the bed). Although the distinction between saltating load and other types of sediment load may be important to those studying the physics of grain movement, most geomorphologists are content to ignore it as a special case.

Bed load is the clastic (particulate) material that moves through the channel fully supported by the channel bed itself. These materials, mainly sand and gravel, are kept in motion (rolling and sliding) by the shear stress acting at the boundary. Unlike the suspended load, the bed-load component is almost always capacity limited (that is, a function of hydraulics rather than supply). A distinction is often made between the bed-material load and the bed load.

Bed-material load is that part of the sediment load found in appreciable quantities in the bed (generally > 0.062 mm in diameter) and is collected in a bed-load sampler. That is, the bed material is the source of this load component and it includes particles that slide and roll along the bed (in bed-load transport) but also those near the bed transported in saltation or suspension. Bed load, strictly defined, is just that component of the moving sediment that is supported by the bed (and not by the flow).

THEORY OF SEDIMENT ENTRAINMENT

At a very simple deterministic level of analysis, a particle of sediment will begin to move when the force of the flowing water applied to it equals its submerged weight. This simple analysis leads to:



Lift & drag forces acting on a submerged particle.

$$\tau_{cr} = K g (\rho_s - \rho) D$$

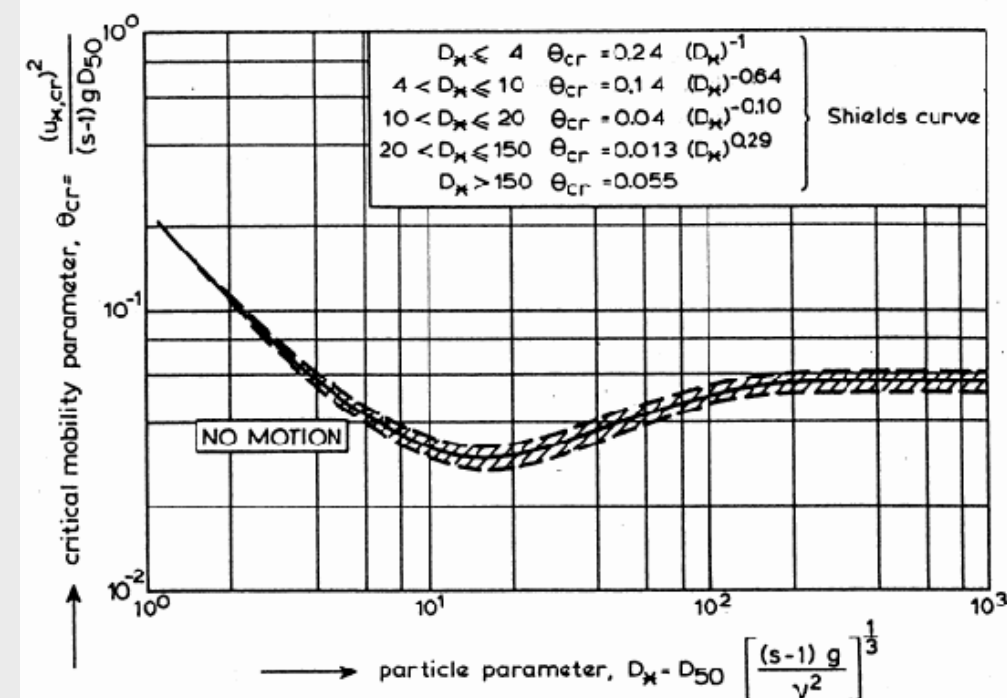
where $K = \frac{\eta}{\tan \phi}$ and $\eta = n D^2$ (a packing coefficient) and ϕ is the internal angle of friction of the sediment. Although this simple analytical approach (called the White analysis, after its originator) is useful because it highlights the general structural relationships

(balance of forces) involved in this problem, it is not of much practical use because it greatly oversimplifies the actual complex forces involved. That is, there is more to this problem of specifying the entrainment conditions than merely balancing mean boundary shear stress and the submerged weight of the particle. Mean boundary shear stress is just one of several impelling forces and the particle submerged weight is just one of several inertial forces. Unfortunately, the other forces are very difficult to characterize in a precise quantitative.

SHIELDS ENTRAINMENT FUNCTION

The most widely used semi-empirical approach to defining the threshold of sediment motion was proposed in the early 1900's by the German physicist Albert F. Shields. Shields (1936) plotted the dimensionless shear stress ($\theta = \frac{\tau_{cr}}{g(\rho_s - \rho)D}$) against the particle Reynolds number ($Re_p = \frac{D}{\delta_0}$) where δ_0 is the thickness of the laminar sublayer. The

dimensionless shear stress in the Shields diagram is commonly termed the *Shields stress* or the *Shields parameter*. Several aspects of the Shields diagram are particularly noteworthy:



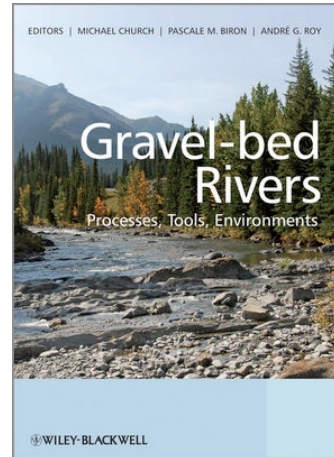
Shields Diagram from Van Rijn (1984).

1. The lowest Shields stress occurs in the sand range (0.06-2.00 mm). Sand is small enough to have small mass but too large for adhesion forces to come into play.
2. Silt/clay, in spite of the smaller size, requires a higher shear stress for motion than sand. Here adhesion forces become overwhelmingly large and bind the sediment together into a mass that is very resistant to erosion.
3. The Shields parameter for gravel is constant at 0.06, implying that Shields stress here becomes a simple function of grain size. This is a quite remarkable finding and allows us, as we will see below, to derive a simple relationship between the size of gravel and the shear stress required to move it.
4. The Shields parameter applies well to natural gravel-bed rivers.

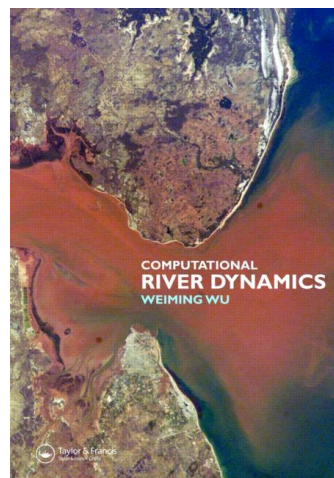
REFERENCES

- Bagnold, R.A., 1980: An empirical correlation of bedload transport rates in flumes and natural rivers. *Proceedings of the Royal Society* 372A, 453-73.
- Colby, B.R. 1963: Fluvial sediments – a summary of source, transportation, deposition, and measurement of sediment discharge. *United States Geological Survey Bulletin* 1181A.
- Degens, E.T., Kempe, S. and Richey, J.E. 1991: Summary: Biogeochemistry of major world rivers. In Degens, E.T., Kempe, S. and Ticey, J.E. (eds), *Biogeochemistry of major world rivers*, SCOPE 42. Chichester: Wiley, 323-47.
- Ham, D.G. and Church, M., 2000: Bed material transport estimated from channel morphodynamics: Chilliwack River, British Columbia. *Earth Surface Processes and Landforms*, 24 (10) 1123-1142.
- Hickin, E.J. 1989: Contemporary Squamish River sediment flux to Howe Sound, British Columbia. *Canadian Journal of Earth Sciences*, 26: 1953-1963.
- Hjulstrom, F. 1935: Studies of the morphological activity of rivers as illustrated by the River Fyris. *Bulletin of the Geological Institute University of Uppsala*, 25, 221-527.
- Meybeck, M. 1976: Total mineral dissolved transport by world major rivers. *Hydrological Sciences Bulletin, International Association of Scientific Hydrology*, 21, 265-84.
- Milliman, J.D. and Meade, R.H. 1983: World-wide delivery of river sediment to the oceans. *Journal of Geology*, 91, 1-21.
- Nordin, C.F. and Beverage, J.P. 1965: Sediment transport in the Rio Grande, New Mexico. *U.S. Geological Survey Professional Paper* 462F, 35.
- Pelpola, C. and Hickin, E.J. 2004: Long-term bed-load transport rate based on air photo and ground-penetrating radar surveys of fan-delta growth, Coast Mountains, British Columbia. *Geomorphology*, 57, 169-181.
- Shields, A. 1936: Anwendung der Ahnlichkeitsmechanik und der Turbulenzforschung auf die Geschiebebewegung. *Mitteilung der preussischen Versuchsanstalt fur Wasserbau und Schiffbau*, 26, Berlin.
- Walling, D.E. and Webb, B.W. 1987: Suspended load in gravel-bed rivers: UK experience: In Thorne, C.R., Bathurst, J.C. and Hey, R.D. (eds), *Sediment transport in gravel-bed rivers*. Chichester: Wiley, 691-723.
- Williams, G.P. 1989: Sediment concentration versus water discharge during single hydrologic events in rivers. *Journal of Hydrology*, 111, 89-106

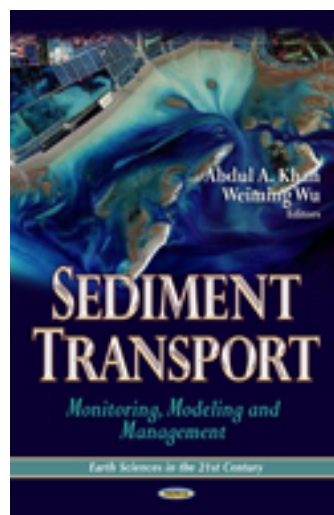
FURTHER READING



Church, Michael; Biron, Pascale M.; Roy, Andre G., eds. *Gravel-Bed Rivers: Processes, Tools, Environments*. Chichester, UK: Wiley. p. 435-463.



W.Wu (2007). *Computational River Dynamics*, Taylor & Francis, UK, 494 p.



A. Khan and W. Wu (eds) (2013). *Sediment Transport: Monitoring, Modeling and Management*, Nova Science Publishers, NY.

Quantitative geomorphology



SECTION 1

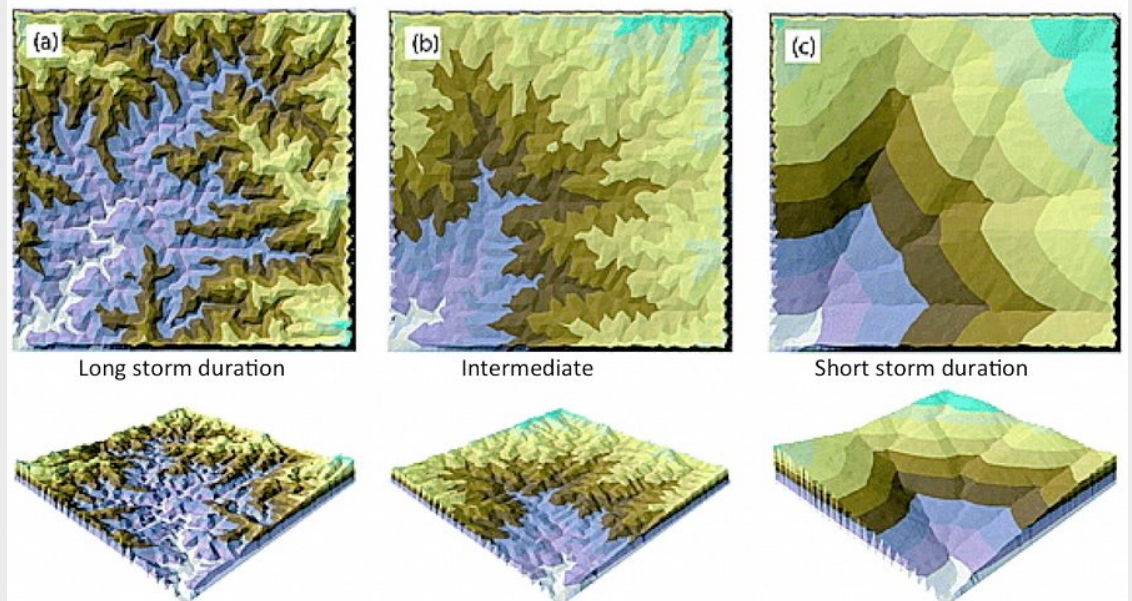
Landscape evolution models overview

KEY POINTS

1. Surface processes models.
2. Hillslope erosion.
3. Soil production.

The development of the **Badlands** model (**Basin and landscape dynamics**) is made in the context of the growing number of landscape evolution models (or surface processes models - SPMs) that have been proposed during the last decades. Many geomorphological applications have demonstrated the usefulness of these models, whose predictions help researchers test simple to complex hypotheses on the nature of landscape evolution. SPMs also provide connection between small-scale, measurable processes and their long-term geomorphic implications (Tucker et al., 2001b). Below, we give a brief overview of SPMs, their history and their conceptual basis.

SURFACE PROCESSES MODELS



Role of storm duration in shaping catchment (Solyom & Tucker, 2004).

The roots of landscape evolution theory can be found in the pioneering work of Gilbert (1877), who proposed a set of hypotheses to relate various landforms to the mechanisms of weathering, erosion and sediment transport. The first quantitative models appeared later in the 1960s (e.g., Culling, 1960; Scheidegger, 1961; Ahnert, 1970; Kirkby, 1971). These models formalize the concepts of Gilbert (1877) to the develop-

Models	Example reference	Note
SIBERIA	Willgoose et al. (1991)	Transport-limited; Channel activator function
DRAINAL	Beaumont et al. (1992)	“Undercapacity” concept
GILBERT	Chase (1992)	Precipiton
DELIM/MARSSIM	Howard (1994)	Detachment-limited; Nonlinear diffusion
GOLEM	Tucker & Slingerland (1994)	Regolith generation; Threshold landsliding
CASCADE	Braun & Sambridge (1997)	Irregular discretization
CAESAR	Coulthard et al. (1996)	Cellular automaton algorithm for 2D flow field
ZSCAPE	Densmore et al. (1998)	Stochastic bedrock landsliding algorithm
CHILD	Tucker & Bras (2000)	Stochastic rainfall
EROS	Crave & Davy (2001)	Modified precipiton
LAPSUS	Schoorl et al. (2002)	Multiple flow directions
APERO/CIDRE	Carretier & Lucaleau (2005)	Single or multiple flow directions
TISC	Garcia-Castellanos (2003)	Lithospheric-scale tectonics
FEM	Simpson & Schlunegger (2008)	Debris flow
FASTSCAPE	Braun & Willet (2013)	Implicit & parallel
LANDLAB	Tucker et al. (2014)	Python software package
CSDMS	http://csdms.colorado.edu/wiki/Main_Page	

ment of hillslope profiles. A few years later, these models were extended to two dimensions, although still focused on hillslope morphology (*e.g.*, Ahnert, 1976; Kirkby, 1986). During the last two decades, as computers continued to get faster, a number of sophisticated numerical SPMs have been developed, mainly focusing on watershed or moun-

tain belt evolution (*e.g.*, Willgoose et al., 1991; Howard, 1994; Tucker and Slingerland, 1997; Braun and Sambridge, 1997; Densmore et al., 1998; Tucker et al., 2001b; Crave and Davy, 2001; Coulthard et al., 2002). Both hillslope and fluvial processes are involved in these models, which differ from each other by the parameterization of these processes and their numerical resolution. For a complete overview of surface processes modeling and the recent SPMs, the reader is referred to the numerous reviews on that topic (Beaumont et al., 1999; Coulthard, 2001; Martin and Church, 2004; Willgoose, 2005; Codilean et al., 2006; Bishop, 2007; Tucker and Hancock, 2010).

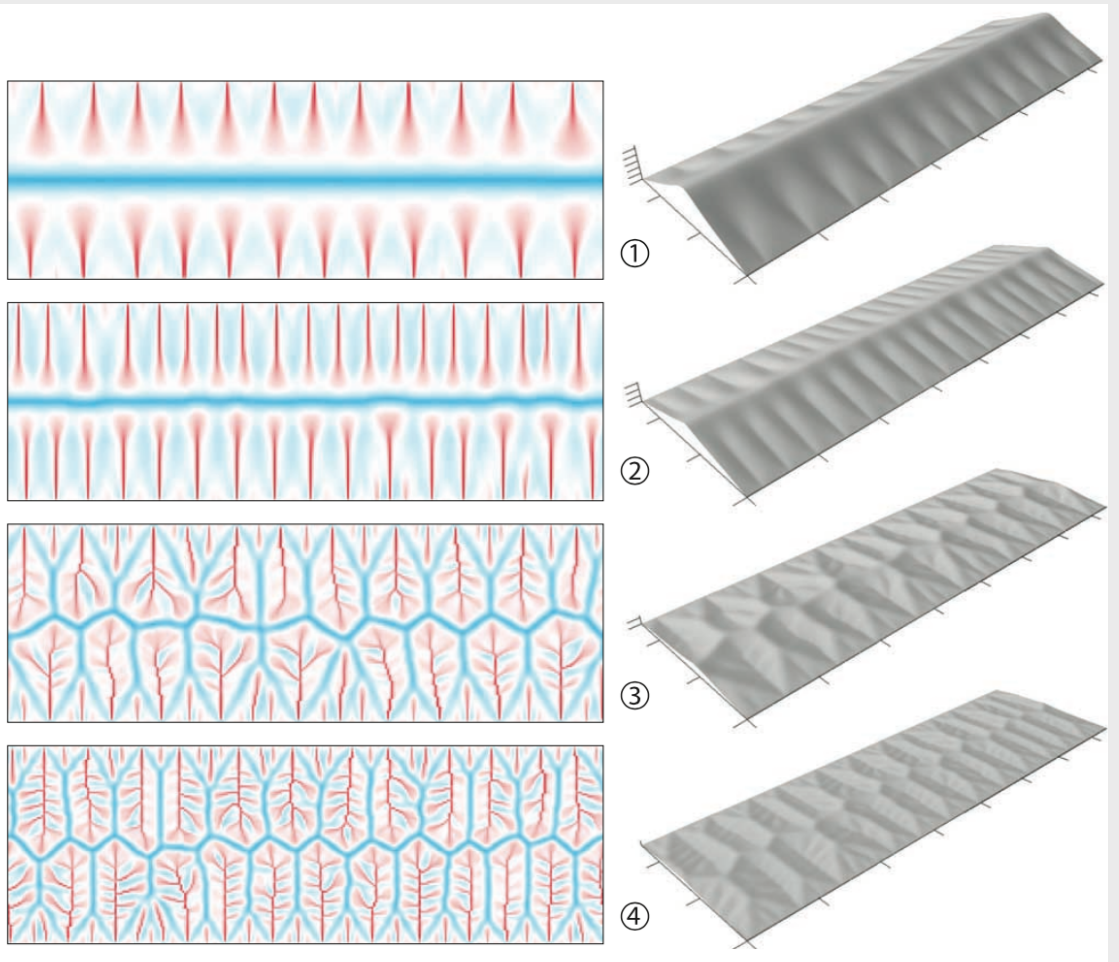
Most of the recent SPMs are still based on the principle that landforms result from a unique suite of surface processes (Roering et al., 2004). For example, channel gradients tend to decrease with increasing drainage area in bedrock rivers because incision is proportional to stream power.

HILLSLOPE: THE DIFFUSION EQUATION

Formulations for hillslope erosion are mainly derived considering hillslope form (*e.g.*, convex, convex-concave, planar). In many SPMs, sediment transport rate on hillslopes is assumed to be equal to a linear function of topographic gradient. Such an expression has its origin in the pioneering studies of convex hillslopes by Davis (1892) and Gilbert (1909). Combined with the application of mass conservation, this leads to the diffusion equation below that describes the rate of elevation

change $\frac{\partial z}{\partial t}$:

$$\begin{aligned}\frac{\partial z}{\partial t} &= - \nabla \cdot \mathbf{q}_s, \\ \mathbf{q}_s &= - K \nabla z, \\ \Leftrightarrow \frac{\partial z}{\partial t} &= K \nabla^2 z\end{aligned}$$



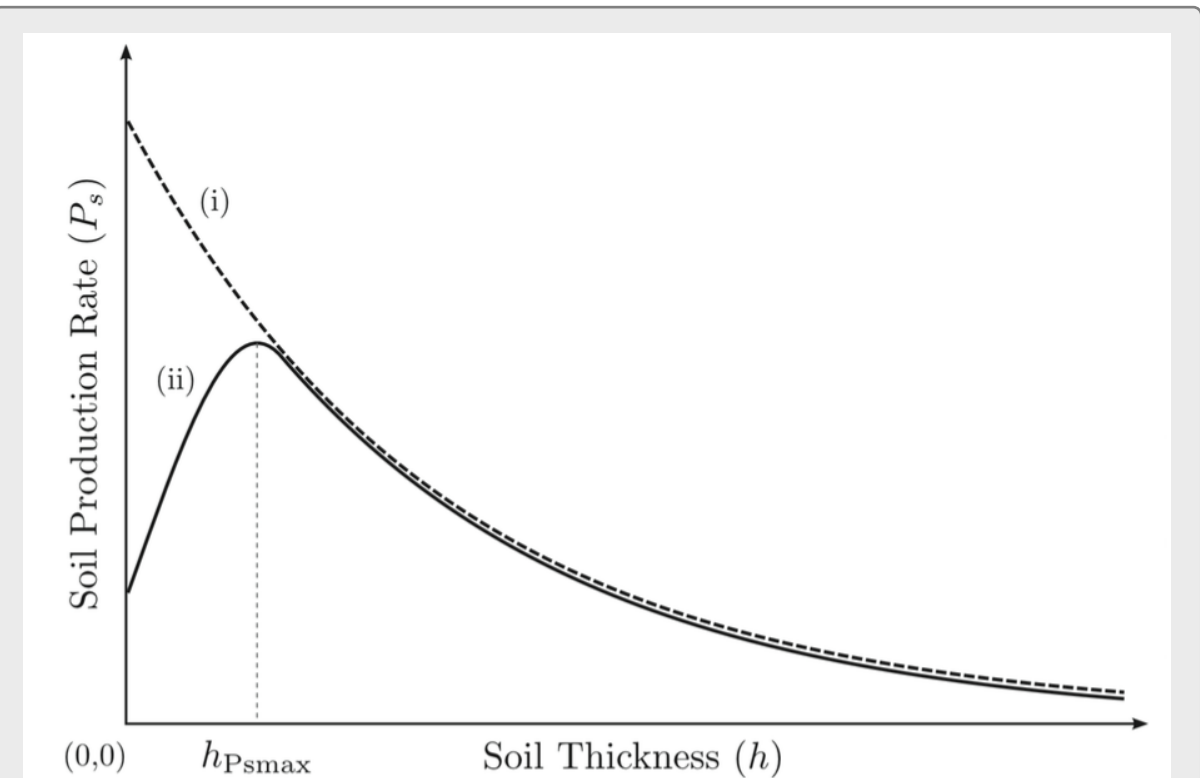
Four representative solutions to topographic evolution showing the variety of observed behavior from Perron et al. (2008). Colors in the image maps (left) show the Laplacian of elevation ($\nabla^2 z$) normalized to the maximum and minimum values in the grid. Concave-up areas (red) are valleys; concave-down areas (blue) are hillslopes. Axis tick intervals in the perspective views (right) are 200 m in the horizontal and 5 m in the vertical. Vertical exaggeration 4X.

where z is the elevation, $\nabla \cdot$ is the spatial divergence operator, ∇z is the topographic gradient (i.e., the local slope), \mathbf{q}_s is the soil flux in the positive direction of ∇z , and K is the hillslope diffusivity.

SOIL PRODUCTION FUNCTIONS

A few modeling studies considered the evolution of soil mantle in addition to the evolution of topographic surface (e.g., Ahnert, 1976; Dietrich et al., 1995; Heimsath et al., 1999; Braun et al., 2001). Soil production, or rock weathering, is the result of a variety of chemical and

mechanical processes. It is, however, difficult for geomorphologists to consider each of these processes separately while studying the form of the landscape. Bedrock weathering rates are thus usually estimated using empirical soil production functions, i.e., relationships between weathering rates and soil depth. A substantial review of the history of soil production functions has been made by Humphreys & Wilkinson (2007). Here again, the roots of soil production functions can be found in Gilbert (1877). This author suggested that a minimum soil cover is needed for bedrock weathering, as soil acts as a reservoir of water essential to weathering processes such as freeze-thaw or solutional processes. At depths beyond which soil production is maximised, soil production is self limiting as thicker soil progressively buffers the underlying bedrock from weathering. This behaviour can be represented by a ‘humped’ function (Cox, 1980) (Figure curve ii). This relationship has been assumed for 100 years, but has not been quantitatively tested un-

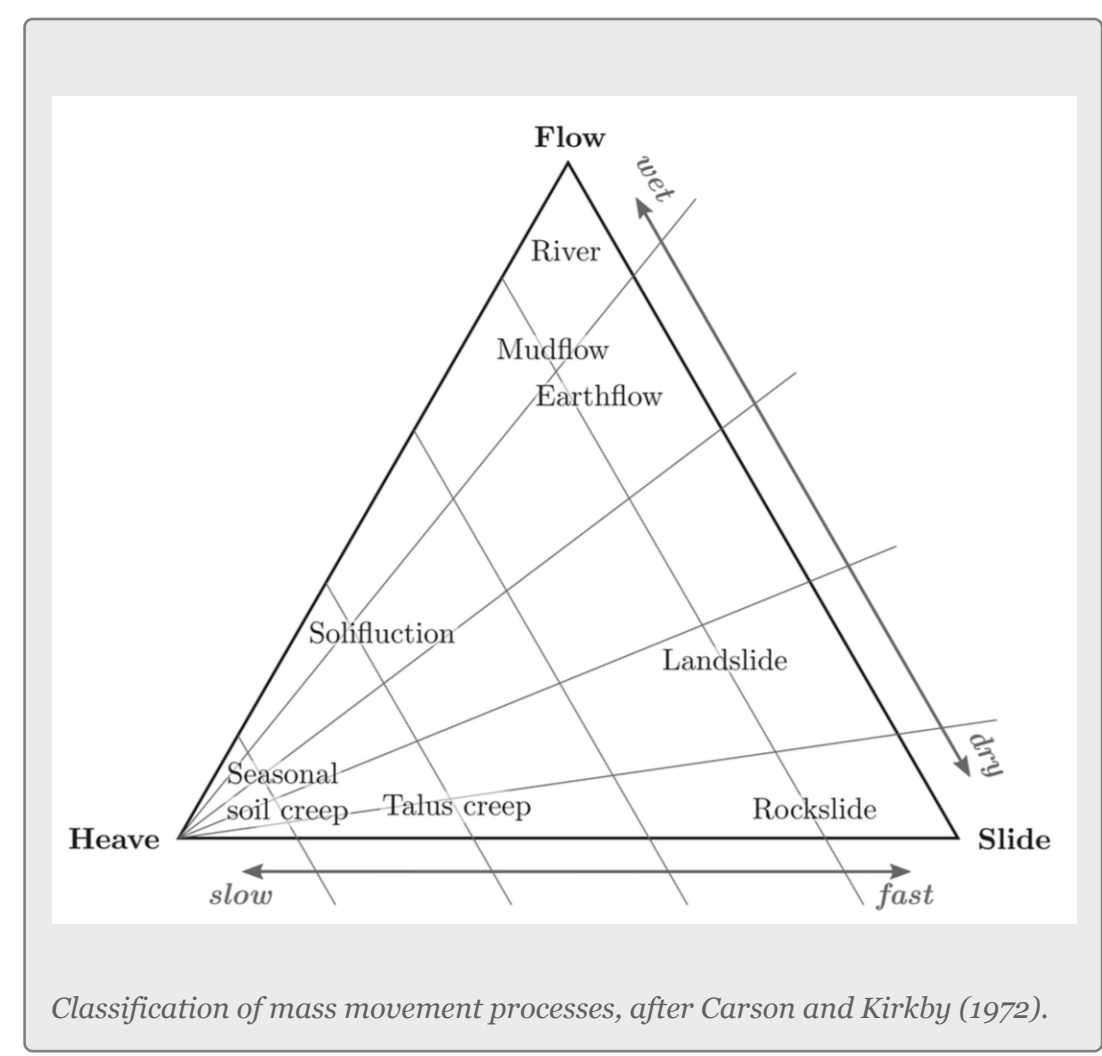


Schematic representation of (i) the exponential soil production function proposed by Dietrich et al. (1995) and Heimsath et al. (1997, 1999), and (ii) the humped soil production function initially proposed by Gilbert (1877), where $h_{P\max}$ corresponds to the optimal depth of soil production. Redrawn from (Humphreys & Wilkinson, 2007).

til recently. Heimsath et al. (1997, 1999) have first applied field methods and cosmogenic dating to hillslopes in northern California to determine soil production rates as a function of soil depth. These observations suggest an exponential decrease in soil production with increasing soil depth (Figure curve i), as proposed earlier by (Dietrich et al., 1995). Both humped and exponential soil production functions are supported at other study sites (*e.g.*, Small et al., 1999; Heimsath et al., 2000; Wilkinson et al., 2005), although unequivocal field evidence for either of these functions is still absent (Wilkinson and Humphreys, 2005).

MODELING SOIL TRANSPORT & HILLSLOPE

Although the linear dependence of soil transport on local slope has been widely assumed (*e.g.*, Ahnert, 1967; Nash, 1980; Dietrich et al., 1995; Fernandes and Dietrich, 1997; Heimsath et al., 1999; Martin, 2000), only a few observations support this relationship (McKean et al., 1993; Small et al., 1999). Moreover, it is well admitted that sediment transport on hillslopes result from a variety of processes (Figure 1.2), such as landsliding, rain-splash, depth-dependent creep, or overland flow (Nemcok et al., 1972; Carson and Kirkby, 1972; Selby, 1993; Hovius et al., 1997; Prosser and Rustomji, 2000). Other transport laws have therefore been proposed. These laws, still based on the process/form principle, state that transport rates depend non-linearly on local slope (*e.g.*, Anderson, 1994; Howard, 1994; Roering et al., 1999), on depth of soil movement (*e.g.*, Selby, 1993; Heimsath et al., 2005; Roering, 2008) and/or on drainage area or overland flow discharge (*e.g.*, Prosser and Rustomji, 2000). A review of many geomorphic transport laws has been made by Dietrich et al. (2003). Recently, some authors have proposed new SPMs using parameterization of soil transport which involves several processes, *i.e.*, in which soil transport on slopes results from the combination of multiple geomorphic transport laws (Schoorl et al., 2000; Braun et al., 2001; Schoorl et al., 2002; Herman and Braun, 2006).



Classification of mass movement processes, after Carson and Kirkby (1972).

In surface processes modeling, a key issue to address is the calibration of the parameters of the transport laws. Most of these laws have only a limited physical basis, and their parameters are calibrated by comparing model predictions and observations (Furbish et al., 2009). These parameters are often assumed constant, although they must certainly vary with material properties, environmental or climatic variables such as rainfall and temperature, and biological activity (Carson and Kirkby, 1972). Calibrated values of these parameters are therefore related to specific environments. For example, Fernandes and Dietrich (1997) and Martin (2000) have synthesized many field-estimates of the diffusion-like coefficient K in the diffusion equation, each related to a specific soil material and climate. The aim of our work is closely related to this calibration issue. By developing the parameterization of soil

transport, our purpose is to remove the climatic dependence from the calibration of the parameters of soil transport laws. Calibrated values could therefore be valid in a larger range of environments, and also in environments that underwent drastic climatic changes.

Note that, beside the surface processes modeling framework discussed so far, a number of alternative hillslope erosion models coexist. Recent studies have proposed a representation of hillslope processes using a stochastic approach (*e.g.*, Tucker and Bradley, 2010), a particle-based approach (*e.g.*, Heimsath et al., 2002; Furbish et al., 2009) or a non-local theory of soil transport (Foufoula-Georgiou et al., 2010; Furbish and Haff, 2010). A number of soil erosion models also emerged in the field of environmental and soil research (Merritt et al., 2003), either empirically-based (*e.g.*, USLE or RUSLE, Renard et al., 1994), or conceptual or physically-based (*e.g.*, WEPP, Laflen et al., 1991). These models have, however, been rarely used by geomorphologists for several reasons (*e.g.*, assumption of constant or static topography, too detailed description of erosion mechanisms to be applied at large spatial and temporal scales).

REFERENCES

- Ahnert, F., 1970. A comparison of theoretical slope models with slopes in the field. *Zeitschrift für Geomorphologie* 9, 88–101.
- Ahnert, F., 1976. Brief description of a comprehensive three-dimensional process-response model of landform development. *Zeitschrift für Geomorphologie* 25, 29–49.
- Anderson, R., 1994. Evolution of the Santa Cruz mountains, California, through tectonic growth and geomorphic decay. *Journal of Geophysical Research* 99, 20161–20179.
- Beaumont, C., Kooi, H., Willett, S., 1999. Coupled tectonic-surface process models with applications to rifted margins and collisional orogens. In: Summerfield, M. (Ed.), *Geomorphology and Global Tectonics*. Wiley, New York, pp. 29–55.
- Bishop, P., 2007. Long-term landscape evolution: linking tectonics and surface processes. *Earth Surface Processes and Landforms* 32 (3), 329–365.
- Braun, J., Heimsath, A. M., Chappell, J., 2001. Sediment transport mechanisms on soil-mantled hillslopes. *Geology* 29 (8), 683–686.
- Braun, J., Sambridge, M., 1997. Modelling landscape evolution on geological time scales: a new method based on irregular spatial discretization. *Basin Research* 9 (1), 27–52.
- Carson, M., Kirkby, M., 1972. *Hillslope form and process*. Cambridge University Press, New York.
- Codilean, A., Bishop, P., Hoey, T. B., 2006. Surface process models and the links between tectonics and topography. *Progress in Physical Geography* 30 (3), 307.
- Coulthard, T., 2001. Landscape evolution models: a software review. *Hydrological Processes* 15, 165–173.
- Coulthard, T. J., Macklin, M. G., Kirkby, M. J., 2002. A cellular model of Holocene upland river basin and alluvial fan evolution. *Earth Surface Processes and Landforms* 27 (3), 269–288.
- Cox, N., 1980. On the relationship between bedrock lowering and regolith thickness. *Earth Surface Processes* 5, 271–274.
- Crave, A., Davy, P., 2001. A stochastic “precipiton” model for simulating erosion/sedimentation dynamics. *Computers and Geosciences* 27 (7), 815–827.
- Culling, W., 1960. Analytical theory of erosion. *Journal of Geology* 68, 336–344.
- Davis, W. M., 1892. The convex profile of badland divides. *Science* 20, 245.
- Densmore, A., Ellis, M., Anderson, R., 1998. Landsliding and the evolution of normal-fault-bounded mountains. *Journal of Geophysical Research* 103, 15203–15219.
- Dietrich, W. E., Bellugi, D., Sklar, L. S., Stock, J., Heimsath, A. M., Roering, J. J., 2003. Geomorphic transport laws for predicting landscape form and dynamics. In: Wilcock, P. R., Iverson, R. M. (Eds.), *Prediction in Geomorphology*. Vol. 135. AGU American Geophysical Union, Washington DC, pp. 103–132.
- Dietrich, W. E., Reiss, R., Hsu, M. L., Montgomery, D. R., 1995. A process-based model for colluvial soil depth and shallow landsliding using digital elevation data. *Hydrological Processes* 9 (3-4), 383–400.
- Fernandes, N., Dietrich, W. E., 1997. Hillslope evolution by diffusive processes: The timescale for equilibrium adjustments. *Water Resources Research* 33 (6), 1307–1318.
- Foufoula-Georgiou, E., Ganti, V., Dietrich, W. E., Jun, 2010. A nonlocal theory of sediment transport on hillslopes. *Journal of Geophysical Research* 115, 1–12.
- Furbish, D. J., Haff, P. K., Jul, 2010. From divots to swales: Hillslope sediment transport across diverse length scales. *Journal of Geophysical Research* 115 (F3), 1–19.

- Furbish, D. J., Haff, P. K., Dietrich, W. E., Heimsath, A. M., Sep. 2009. Statistical description of slope-dependent soil transport and the diffusion-like coefficient. *Journal of Geophysical Research* 114 (1), 1–19.
- Gilbert, G., 1877. Report on the Geology of the Henry Mountains. U.S. Geological and Geo-logical Survey of the Rocky Mountain Region, Washington, D.C.
- Gilbert, G., 1909. The convexity of hilltops. *Journal of Geology* 17, 344–350.
- Heimsath, A., Chappell, J., Dietrich, W., Nishiizumi, K., Finkel, R., 2000. Soil production on a retreating escarpment in southeastern Australia. *Geology* 28 (9), 787.
- Heimsath, A., Dietrich, W., Nishiizumi, K., Finkel, R., 1997. The soil production function and landscape equilibrium. *Nature* 388 (6640), 358–361.
- Heimsath, A., Dietrich, W. E., Nishiizumi, K., Finkel, R. C., 1999. Cosmogenic nuclides, topo- graphy, and the spatial variation of soil depth. *Geomorphology* 27, 151–172.
- Heimsath, A. M., Chappell, J., Spooner, N. a., Questiaux, D. G., 2002. Creeping soil. *Geology* 30 (2), 111.
- Heimsath, A. M., Furbish, D. J., Dietrich, W. E., 2005. The illusion of diffusion: Field evidence for depth-dependent sediment transport. *Geology* 33 (12), 949.
- Herman, F., Braun, J., 2006. A parametric study of soil transport mechanisms. *GSA Special Papers* 398 (11), 191.
- Hovius, N., Stark, C., Allen, P., 1997. Sediment flux from a mountain belt derived from landslide mapping: *Geology*. *Geology* 25, 231–234.
- Howard, A., 1994. A detachment limited model of drainage basin evolution. *Water Resources Research* 30, 2261–2285.
- Humphreys, G. S., Wilkinson, M. T., Apr. 2007. The soil production function: A brief history and its rediscovery. *Geoderma* 139 (1-2), 73–78.
- Kirkby, M., 1986. A two-dimensional simulation model for slope and stream evolution. In: Ab- rahams, A. (Ed.), *Hillslope processes*: Winchester, Mass. Allen and Unwin, pp. 203– 222.
- Kirkby, M. J., 1971. Hillslope process-response models based on the continuity equation. *Inst. Brit. Geogr., Spec. Publ.* 3, 15–30.
- Laflen, J., Lane, L., Foster, G., 1991. WEPP: A new generation of erosion prediction technology. *Journal of Soil and Water Conservation* 46, 34–38.
- Martin, Y., 2000. Modelling hillslope evolution: linear and nonlinear transport relations. *Geo- morphology*.
- Martin, Y., Church, M., 2004. Numerical modelling of landscape evolution: geomorphological per- spectives. *Progress in Physical Geography* 28 (3), 317 – 339.
- McKean, J., Dietrich, W., Finkel, R., Southon, J., Caffee, M., 1993. Quantification of soil production and downslope creep rates from cosmogenic ^{10}Be accumulations on a hillslope profile. *Geology* 21 (4), 343.
- Merritt, W., Letcher, R., Jakeman, A., Oct. 2003. A review of erosion and sediment transport mod- els. *Environmental Modelling & Software* 18 (8-9), 761–799.
- Nash, D., 1980. Forms of bluffs degraded for different lengths of time in Emmet County, Michigan, USA. *Earth Surface Processes and Landforms* 5, 331–345.
- Nemcok, A., Pasek, J., Rybar, J., Oct. 1972. Classification of landslides and other mass move- ments. *Rock Mechanics and Rock Engineering* 4 (2), 71–78.
- Prosser, I., Rustomji, P., 2000. Sediment transport capacity relations for overland flow. *Progress in Physical Geography* 24, 179–193.
- Renard, K., Laflen, J., Foster, G., McCool, D., 1994. The revised universal soil loss equation. In: Lad, R. (Ed.), *Soil Erosion: Research Methods*. pp. 105–126.
- Roering, J., Kirchner, J., Dietrich, W., 1999. Evidence for nonlinear, diffusive sediment transport on hillslopes and implications for landscape morphology. *Water Resources Research* 35 (3), 853– 870.
- Roering, J. J., Dec. 2004. Soil creep and convex-upward velocity profiles: theoretical and experi- mental investigation of disturbance-driven sediment transport on hillslopes. *Earth Surface Proc- esses and Landforms* 29 (13), 1597–1612.
- Roering, J. J., 2008. How well can hillslope evolution models “explain” topography? Simulating soil transport and production with high-resolution topographic data. *Geological Society of America Bul- letin* 120 (9), 1248.
- Scheidegger, A., 1961. Mathematical models of slope development. *Geological Society of America Bulletin* 72, 37–50.
- Schoorl, J. M., Sonneveld, M. P. W., Veldkamp, A., 2000. Three-dimensional landscape process modellling: the effect of dem resolution. *Earth Surface Processes and Landforms* 25, 1025–1034.
- Schoorl, J. M., Veldkamp, A., Bouma, J., 2002. Modeling Water and Soil Redistribution in a Dy- namic Landscape Context. *Soil Science Society of America Journal* 66, 1610–1619.
- Selby, M., 1993. *Hillslope materials and processes*, 2nd Edition. Oxford University Press.
- Small, E., Anderson, R., Hancock, G., 1999. Estimates of the rate of regolith production using ^{10}Be and ^{26}Al from an alpine hillslope. *Geomorphology* 27, 131–150.

Tucker, G. E., Bradley, D. N., Mar. 2010. Trouble with diffusion: Reassessing hillslope erosion laws with a particle-based model. *Journal of Geophysical Research* 115, 1–12.

Tucker, G. E., Hancock, G., 2010. Modelling landscape evolution. *Earth Surface Processes and Landforms* 35 (1), 28–50.

Tucker, G. E., Lancaster, S. T., Gasparini, N. M., Bras, R. L., Rybarczyk, S. M., 2001a. An object-oriented framework for distributed hydrologic and geomorphic modeling using triangulated irregular networks. *Computers & Geosciences* 27, 959–973.

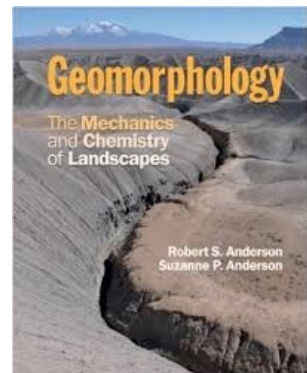
Tucker, G. E., Lancaster, S. T., Gasparini, N. M., L, R., 2001b. The channel-hillslope integrated landscape development (CHILD) model. In: Harmon, R. S., Doe, W. (Eds.), *Landscape Erosion and Evolution Modeling*, iii Edition. Kluwer Academic/Plenum, New York, Ch. 12, pp. 349–388.

Wilkinson, M., Humphreys, G., 2005. Exploring pedogenesis via nuclide-based soil production rates and OSL-based bioturbation rates. *Australian Journal of Soil Research* 43 (6), 767–779.

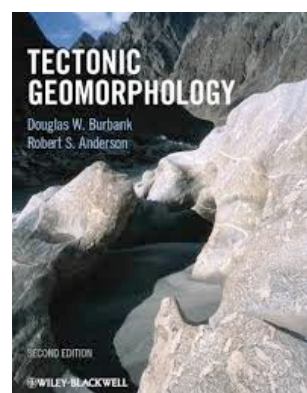
Willgoose, G., 2005. Mathematical Modeling of Whole Landscape Evolution. *Annual Review of Earth and Planetary Sciences* 33 (1), 443–459.

Willgoose, G., Bras, R. L., Rodriguez-Iturbe, I., 1991. A Coupled Channel Network Growth and Hillslope Evolution Model 1. Theory. *Water Resources Research* 27 (7), 1671–1684.

FURTHER READING



Anderson, R. S., & Anderson, S. P. (2010). *Geomorphology: the mechanics and chemistry of landscapes*. Cambridge University Press.



Burbank, D. W., & Anderson, R. S. (2011). *Tectonic geomorphology*. John Wiley & Sons.

SECTION 2

Badlands: general equations

KEY POINTS

1. Empirical formalism for regolith production.
2. Overland flow models.
3. Diffusion laws for hillslope processes.

CONTINUITY OF MASS

CASE 1: NO REGOLITH AND ELEVATION CHANGE

In the simplest case where the model does not distinguish between a regolith layer and the bedrock underneath, the mass continuity equations for a column of soil or rock is expressed as:

$$\frac{\partial z}{\partial t} = U - \nabla \cdot \mathbf{q}_s$$

where the elevation z (m) is measured vertically, \mathbf{q}_s is the total downhill soil flux, and $\nabla \cdot$ is the spatial divergence operator and U (m/yr) is a source term that can either represent the rate of incision of channel streams at the hillslope boundaries or uniform uplift. This is one of several variations; for discussion of others, see Tucker and Hancock (2010).

CASE 2: SOIL THICKNESS AND ELEVATION CHANGE

In case where the model distinguishes between a regolith layer and the bedrock underneath, and considering no aeolian input nor significant loss by dissolution, the local rate of soil thickness change, $\frac{\partial h}{\partial t}$ (m/yr), is determined by the balance between soil production and soil transport:

$$\rho_s \frac{\partial h}{\partial t} = \rho_r P_s - \rho_s \nabla \cdot \mathbf{q}_s \Leftrightarrow \frac{\partial h}{\partial t} = \kappa P_s - \nabla \cdot \mathbf{q}_s$$

where soil thickness h (m) is measured vertically, ρ_r is rock density, ρ_s is soil bulk density (κ is the ratio of rock density to soil density), P_s is the rate of bedrock weathering or soil production (m/yr), \mathbf{q}_s is the total downhill soil flux, and $\nabla \cdot$ is the spatial divergence operator. Soil bulk (dry) density of most soils varies within the range of 1.1-1.6 g/cm^3 , while the density of soil particles (i.e., the bedrock weathered material) has a short range of 2.6-2.7 g/cm^3 in most mineral soils (Hillel, 1980). A value of $\kappa \sim 2$ is therefore acceptable.

The local rate of surface elevation change, $\frac{\partial z}{\partial t}$ (m/yr), is related to the rate of soil thickness change:

$$\frac{\partial z}{\partial t} = \frac{\partial h}{\partial t} - \kappa P_s + U$$

where U (m/yr) is a source term that can either represent the rate of incision of channel streams at the hillslope boundaries or uniform uplift.

PARAMETRIZATION OF PROCESS MODULES

To describe the rates of soil production and soil transport, we mainly follow an empirical soil production law and six empirical or process-based transport laws. Note that landslides and other rapid processes are not considered here.

SOIL PRODUCTION FUNCTION

Bedrock weathering is modeled using the exponential soil production function used by Heimsath et al. (1997, 1999). The rate of weathering P_s (m/yr) is given by

$$P_s = P_0 e^{-h/h_0}$$

where P_0 is expressed in m/yr and h_0 (m) is a characteristic soil depth at which $P_s = (1/e)P_0$.

This soil production law has been calibrated at different sites (in northern California and southern Australia) using both soil thickness and cosmogenic radionucleides (CRN) measurements (Heimsath et al., 1999, 2000). For these sites, the authors reported values of P_0 between $5 \cdot 10^{-5}$ and $8 \cdot 10^{-5}$ m/yr and a value of $h_0 \simeq 0.5m$.

OVERLAND FLOW: DETACHMENT-LIMITED MODEL

In this case, the soil transport rate per unit width by flowing water, \mathbf{q}_r , is modeled as a power function of topographic gradient ∇z and surface water discharge per unit width q_w (m^2/yr):

$$\mathbf{q}_r = -\kappa_r (q_w)^m (\nabla z)^n$$

Note that $(\nabla z)^n$ is short-hand for $\|\nabla z\|^{n-1} \nabla z$, as soil flux is oriented in the direction of the topographic gradient (like for the other transport laws).

This detachment-limited incision rate, which is calculated as a power-law function of fluvial discharge only applies where channel slope is positive, (e.g., Howard, 1994; Whipple and Tucker, 1999):

$$\frac{\partial z}{\partial t} = -\kappa_r (q_w)^m (\nabla z)^n$$

This expression corresponds to a simplified form of the usual expression of sediment transport by water flow (Howard, 1980), in which the transport rate is assumed to be equal to the local carrying capacity, which is itself a function of boundary shear stress or stream power per unit width (Tucker and Hancock, 2010). We consider additionally no threshold for particle entrainment. The exponents m and n have values between 1 and 2 (Willgoose et al., 1991; Howard et al., 1994; Tucker and Bras, 1998; Prosser and Rustomji, 2000; Bogaart et al., 2003a).

OVERLAND FLOW: UNDER-CAPACITY MODEL

River channels have a sediment-carrying capacity (*i.e.*, sediment volume that can be carried per unit time), \mathbf{q}_e , which is proportional to local slope, S , and the local discharge q_w :

$$\mathbf{q}_e = -\kappa_f S q_w$$

where κ_f is a constant (m/yr) that varies mostly with climate and precipitation rate (with higher κ_f values corresponding to a higher precipitation rate).

Following the so-called “under-capacity” model for fluvial erosion and transport that is used within Cascade (Braun and Sambridge, 1997), we assume that a river channel will erode or deposit depending mainly on the relative value of sediment load, q_r , compared to river sediment carrying capacity q_e . Where sediment load is smaller than the river capacity, erosion takes place, at a rate set by:

$$\frac{\partial h}{\partial t} = \left(\frac{q_r - q_e}{\omega_c L_a} \right) \quad \text{if } h > h_0$$

$$\frac{\partial h}{\partial t} = \left(\frac{q_r - q_e}{\omega_c L_b} \right) \quad \text{if } h \leq h_0$$

where (L_a, L_b) is a length scale characterizing the erodibility of alluvial and bedrock respectively (Beaumont et al., 1999) (with higher (L_a, L_b) values corresponding to more resistant rocks). ω_c is the river channel width, which is assumed to be proportional to the local discharge (e.g., Leopold and Maddock, 1953):

$$\omega_c = \beta_c q_w^{\alpha_c}$$

Where sediment load exceeds capacity, deposition takes place at a rate set by

$$\frac{\partial h}{\partial t} = \frac{q_e - q_r}{\Omega}$$

with Ω the surface area attached to each node and defined by the spatial discretization.

HILLSLOPE: SIMPLE CREEP OR LINEAR DIFFUSION

The parameterization of soil transport used here includes the widely-used transport law which states that transport rate depends linearly on topographic gradient. As pointed out by Fernandes & Dietrich (1997), this law —here termed as ‘simple creep’— has in fact been used to represent a variety of transport processes such as creep (e.g., Culling, 1963; Armstrong, 1987), biogenic activity (e.g., Dietrich et al., 1987; He-

imsath et al., 1999, 2002) or rain splash (e.g., De Ploey and Savat, 1968; Dunne et al., 2010). Downslope simple creep is commonly regarded as operating in a shallow superficial layer (Braun et al., 2001) and is defined as:

$$\mathbf{q}_d = -\kappa_d \nabla z$$

Note that because of the multi-process parameterization of soil transport, the coefficient κ_d is also scale-dependent (Dietrich et al., 1995), like the “ κ ” scale parameters of the other transport laws included in our model.

HILLSLOPE: NON-LINEAR DIFFUSION

The actual relevance of an equation such as the simple creep in modeling hillslope processes is currently subject to scientific debate (see e.g., Tucker and Bradley, 2010; Foufoula-Georgiou et al., 2010). Often, an alternative mathematical equation has been invoked to account for non-linear dependency of sediment fluxes on terrain slope instead of the linear relation proposed above, such as (e.g., Roering et al., 1999):

$$\mathbf{q}_{nd} = -\frac{\kappa_{nd} \nabla z}{1 - \left(\frac{|\nabla z|}{S_c} \right)^2}$$

which is used for values of ∇z smaller than the critical slope S_c . Since $\lim_{\nabla z \rightarrow S_c} \mathbf{q}_{nd} = \infty$, as the local slope increases, it tends asymptotically to the value S_c without overcoming it.

HILLSLOPE: DEPTH-DEPENDENT CREEP

Beside linear creep, a few field observations but numerous laboratory and modeling studies have supported depth-dependent, viscous-like flow of soil (e.g., Ahnert, 1967; Selby, 1993; Braun et al., 2001; Furbish and Fagherazzi, 2001; Heimsath et al., 2005; Roering, 2008). The general expression for depth-dependent creep is given by:

$$\mathbf{q}_{dd} = -\kappa_{dd} h^p (\nabla z)^l$$

Different authors have provided different values for the soil thickness and topographic gradient exponents. For example, Heimsath et al. (2005) used $p = l = 1$, although, generally, the velocity of soil displacement declines exponentially with depth (Roering, 2004). Due to a lack of constraints, Braun et al. (2001) have adopted values from Manning's equation for liquid flow ($p = 1.67$ and $l = 0.5$), which is consistent with constrained values obtained by Herman and Braun (2006) (p ranges from 1.5 to 2.0 and l ranges from 0.5 to 1.0).

REFERENCES

- Ahnert, F., 1967. The role of the equilibrium concept in the interpretation of landforms of fluvial erosion and deposition. In: Macar, P. (Ed.), *L'évolution des versants*. University of Liège, Liège, pp. 23–41.
- Armstrong, A., 1987. Slopes, boundary conditions, and the development of convexo-concave forms—some numerical experiments. *Earth Surface Processes and Landforms* 12 (1), 17–30.
- Beaumont, C., Kooi, H., Willett, S., 1999. Coupled tectonic-surface process models with applications to rifted margins and collisional orogens. In: Summerfield, M. (Ed.), *Geomorphology and Global Tectonics*. Wiley, New York, pp. 29–55.
- Bogaart, P. W., Tucker, G. E., Vries, J. J. D., 2003a. Channel network morphology and sediment dynamics under alternating periglacial and temperate regimes: a numerical simulation study. *Geomorphology* 54, 257 – 277.
- Braun, J., Heimsath, A. M., Chappell, J., 2001. Sediment transport mechanisms on soil-mantled hillslopes. *Geology* 29 (8), 683–686.
- Braun, J., Cambridge, M., 1997. Modelling landscape evolution on geological time scales: a new method based on irregular spatial discretization. *Basin Research* 9 (1), 27–52.
- Crave, A., Davy, P., 2001. A stochastic “precipiton” model for simulating erosion/sedimentation dynamics. *Computers and Geosciences* 27 (7), 815–827.
- Culling, W. E. H., 1963. Soil creep and the development of hillside slopes. *The Journal of Geology* 71 (2), 127–161.
- De Ploey, J., Savat, J., 1968. Contribution à l'étude de l'érosion par le splash. *Zeitschrift für Geomorphologie* 12, 174–193.
- Dietrich, W., Reneau, S., Reneau, C., 1987. Overview: 'Zero-Order Basins' and Problems of Drainage Density, Sediment Transport and Hillslope Morphology. In: *Erosion and Sedimentation in the Pacific Rim*. IAHS Publication No. 165. International Association of Hydrological Sciences, Washington, DC, pp. 27–37.
- Dietrich, W. E., Reiss, R., Hsu, M. L., Montgomery, D. R., 1995. A process-based model for colluvial soil depth and shallow landsliding using digital elevation data. *Hydrological Processes* 9 (3-4), 383–400.
- Dunne, T., Malmon, D. V., Mudd, S. M., Jan. 2010. A rain splash transport equation assimilating field and laboratory measurements. *Journal of Geophysical Research* 115 (F1), 1–16.
- Fernandes, N., Dietrich, W. E., 1997. Hillslope evolution by diffusive processes: The timescale for equilibrium adjustments. *Water Resources Research* 33 (6), 1307–1318.
- Foufoula-Georgiou, E., Ganti, V., Dietrich, W. E., Jun. 2010. A nonlocal theory of sediment transport on hillslopes. *Journal of Geophysical Research* 115, 1–12.
- Furbish, D. J., Fagherazzi, S., 2001. Stability of creeping soil and implications for hillslope evolution. *Water Resources* 37 (10), 2607–2618.
- Heimsath, A., Chappell, J., Dietrich, W., Nishiizumi, K., Finkel, R., 2000. Soil production on a re-treating escarpment in southeastern Australia. *Geology* 28 (9), 787.
- Heimsath, A., Dietrich, W., Nishiizumi, K., Finkel, R., 1997. The soil production function and landscape equilibrium. *Nature* 388 (6640), 358–361.
- Heimsath, A., Dietrich, W. E., Nishiizumi, K., Finkel, R. C., 1999. Cosmogenic nuclides, topography, and the spatial variation of soil depth. *Geomorphology* 27, 151–172.
- Heimsath, A. M., Chappell, J., Spooner, N. a., Questiaux, D. G., 2002. Creeping soil. *Geology* 30 (2), 111.
- Heimsath, A. M., Furbish, D. J., Dietrich, W. E., 2005. The illusion of diffusion: Field evidence for depth-dependent sediment transport. *Geology* 33 (12), 949.
- Herman, F., Braun, J., 2006. A parametric study of soil transport mechanisms. *GSA Special Papers* 398 (11), 191.
- Hillel, D., 1980. *Fundamentals of soil physics*. Academic Press, New-York.
- Howard, A., 1980. Thresholds in river regimes. In: Coates, D. R., Vitek, J. D. (Eds.), *Thresholds in Geomorphology*. George Allen & Unwin, London, pp. 227–258.
- Howard, A., 1994. A detachment limited model of drainage basin evolution. *Water Resources Research* 30, 2261–2285.
- Leopold, L. B., and T. Maddock (1953), The hydraulic geometry of stream channels and some physiographic implications, *Geol. Surv. Prof. Pap.*, 252.

Prosser, I., Rustomji, P., 2000. Sediment transport capacity relations for overland flow. *Progress in Physical Geography* 24, 179–193.

Roering, J., Kirchner, J., Dietrich, W., 1999. Evidence for nonlinear, diffusive sediment transport on hillslopes and implications for landscape morphology. *Water Resources Research* 35 (3), 853–870.

Roering, J. J., Dec. 2004. Soil creep and convex-upward velocity profiles: theoretical and experimental investigation of disturbance-driven sediment transport on hillslopes. *Earth Surface Processes and Landforms* 29 (13), 1597–1612.

Roering, J. J., 2008. How well can hillslope evolution models “explain” topography? Simulating soil transport and production with high-resolution topographic data. *Geological Society of America Bulletin* 120 (9), 1248.

Selby, M., 1993. Hillslope materials and processes, 2nd Edition. Oxford University Press.

Tucker, G. E., Bradley, D. N., Mar. 2010. Trouble with diffusion: Reassessing hillslope erosion laws with a particle-based model. *Journal of Geophysical Research* 115, 1–12.

Tucker, G. E., Bras, R. L., 1998. Hillslope processes, drainage density, and landscape morphology. *Water Resources Research* 34 (10), 2751–2764.

Tucker, G. E., Hancock, G., 2010. Modelling landscape evolution. *Earth Surface Processes and Landforms* 35 (1), 28–50.

Whipple, K., Tucker, G., 1999. Dynamics of the stream-power river incision model: Implications for height limits of mountain ranges, landscape response timescales, and research needs. *Journal of Geophysical Research* 104 (B8), 17661–17.

Whipple, K., Tucker, G. E., 2002. Implications of sediment-flux-dependent river incision models for landscape evolution. *Journal of Geophysical Research* 107 (2039), 10–1029.

Willgoose, G., Bras, R. L., Rodriguez-Iturbe, I., 1991. A Coupled Channel Network Growth and Hillslope Evolution Model 1. Theory. *Water Resources Research* 27 (7), 1671–1684.

SECTION 3

Badlands: spatial and temporal framework

KEY POINTS

1. Spatial framework, finite volume approach.
2. Parallelization strategy.
3. Temporal framework.

SPATIAL FRAMEWORK

Equations detailed in previous section describe the evolution of soil thickness and surface elevation. However, solving these partial differential equations (PDEs) is non-trivial and numerical methods are needed to perform their integration in space and time (for a given set of initial and boundary conditions). This step requires the discretization of the terrain surface, $z(x, y)$, and soil thickness, $h(x, y)$, into a finite number of ‘hillslope elements’, *i.e.*, a lattice of connected points (x_i, y_i) and their associated cells (*i.e.*, the part of the hillslope they represent) at which the solution of the PDEs is calculated. Here, we describe how the topography is discretized in **Badlands** and how the continuity of mass is applied within each element.

DELAUNAY TRIANGULATION AND VORONOI DIAGRAM

Here, we choose to use an irregular spatial discretization scheme similar to the CASCADE (Braun and Sambridge, 1997) and CHILD (Tucker et al., 2001a,b) models to numerically solve the geomorphic equations. The computational mesh is created in three stages: (1) The 2D planimetric space is first discretized as a set of points in any arbitrary configuration, (2) these points are then connected using the Delaunay triangulation (Voronoi, 1908; Delaunay, 1934) to form the nodes of a Triangulated Irregular Network (TIN), and (3) the Voronoi diagram, which corresponds to the dual graph of the Delaunay’s TIN, is constructed. Initial values of surface elevation and soil thickness are then assigned to each node. These values will be updated every time step of a **Badlands** simulation.

The Delaunay triangulation and the Voronoi tessellation are well established in the field of computational geometry (*e.g.*, Fortune, 1992; Sambridge et al., 1995; Du, 1996). The Delaunay triangulation of a set of irregularly spaced points may be defined as the unique triangulation for which the circles passing through the three vertices of each triangle do not contain any other node. Unlike other triangulation methods, this

APPLICATION OF THE FINITE-VOLUME APPROACH

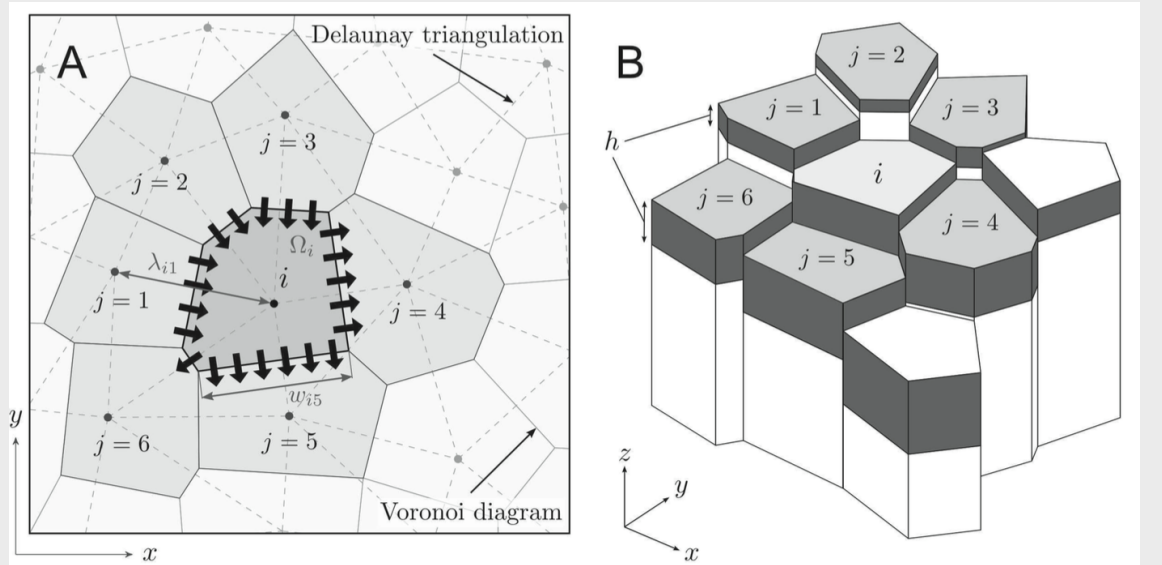
As pointed out by Tucker et al. (2001b), the dual Delaunay-Voronoi framework lends itself to a numerical solution of the continuity equation using the Finite-Volume (FV) approach (Eymard et al., 2000). Applying this approach in our two-dimensional problem consists of integrating the continuity equation over small areas ('finite-volume' cells) surrounding the nodes of the mesh, which here correspond to the Voronoi cells associated to each node. Hereafter, we illustrate the application of the FV method to the node i and its associated Voronoi cell of surface area Ω_i . Using the divergence theorem, the integral over Ω_i of the divergence of the soil flux, $\nabla \cdot \mathbf{q}_s$, can be expressed as the integral of the soil fluxes at the boundary of the Voronoi cell:

$$\iint_{\Omega_i} \nabla \cdot \mathbf{q}_s d\Omega_i = \oint_{w_i} \hat{\mathbf{n}} \cdot \mathbf{q}_s dw_i \simeq \sum_{j=1}^{nb_i} w_{ij} q_{s,ij}$$

where w_i is the total length of the boundary of the Voronoi cell, $\hat{\mathbf{n}}$ is the unit vector normal to the boundary and pointing outward, nb_i is the number of natural neighbours connected to the node i , w_{ij} is the width of the edge shared by adjacent Voronoi cells associated to the node i and its neighbour j , and $q_{s,ij}$ is the total bulk volumetric soil flux across this edge per unit width.

The flux $q_{s,ij}$ is calculated by summing the fluxes defined in previous section, we note that this flux depends on the local topographic gradient across -and normal to- the shared Voronoi edge between the nodes i and j . This gradient is approximated as the topographic gradient between the nodes themselves:

$$\|(\nabla z)_{ij}\| \simeq S_{ij} = \frac{z_j - z_i}{\lambda_{ij}}$$



A mesh sample illustrating the discretization of the hillslope landscape in Badlands. A. Planimetric view showing the mesh nodes (points), the edges of the Delaunay triangles (dashed gray lines) connecting the nodes, and the edges of the corresponding Voronoi cells (plain lines). The thick arrows illustrate the fluxes - more precisely, their normal component - across the Voronoi polygon edges shared by the node i and its 'natural neighbours'. As examples, Ω_i is the area of the Voronoi cell of the node i ; λ_{i1} is the planimetric distance between i and its 1st neighbour; and w_{i5} is the width of the Voronoi edge between the node i and its 5th neighbour (the order of the neighbours doesn't have any importance here). B. 3D representation of a subset of the Voronoi diagram showing the average elevation (height of the 'columns') and the average soil thickness (depth of the dark-gray volumes) associated to each Voronoi cell.

triangulation has the useful property of minimizing the maximum internal angles, thus providing the most 'equable' triangulation of the original set of points. In the Delaunay's TIN, each node is connected to a set of neighbours called the 'natural neighbours'. Its dual Voronoi diagram may be defined as the set of contiguous polygons (cells) formed by intersecting the perpendicular bisectors of the Delaunay triangles. The Voronoi cell about a node is the region of the plane that is closest to the node; it may be regarded as the 'neighbourhood' of the node. To build the mesh in **Badlands**, we use the Triangle implementation from Shewchuk of the Delaunay-Voronoi meshing algorithms.

where z_i and z_j are the surface elevation associated to the nodes i and j , respectively, and λ_{ij} is the planimetric distance between these nodes.

Considering the downslope movement of soil, $q_{s,ij}$ is positive if the net soil flux is from i to j , and negative if the net flux is from j to i . Note also that FV methods are conservative, *i.e.*, that the flux entering (or leaving) a given cell equals the flux leaving (or entering) the adjacent cell ($q_{s,ij} = -q_{s,ji}$). Finally, integrating both sides of the continuity equation over Ω_i gives:

$$\frac{dh_i}{dt} = \kappa P_{s,i} - \frac{1}{\Omega_i} \left(\sum_{j=1}^{nb_i} w_{ij} q_{s,ij} \right)$$

Intuitively, this equation simply states that a non-zero net soil flux out of the Voronoi cell surrounding the node i would result in a general decrease of soil thickness within this cell if the net flux is not balanced by the rate of soil production (inversely, a non-zero net flux entering the cell will always result in accumulation of soil within the cell). Note that in FV applications, the cells -and not the nodes of the mesh- are the primitive elements of the spatial discretization. Because the soil fluxes acting inside the cells are not considered, by using the divergence theorem it is only possible to describe the average rate of soil removal or accumulation, dh/dt , within each cell. When mentioning values of soil thickness, h_i , and surface elevation, z_i , assigned to the node i , we thus refer to the averages over the corresponding Voronoi cell.

NODES ORDERING

Key to the model is to find the order in which one must go through the nodes to compute discharge by adding progressively the contribution of each node to the river discharge (or its contributing area to the total drainage area). To perform this operation, we assume that water goes down the path of the steepest slope (O'Callaghan and Mark, 1984; Gal-lant and Wilson, 2000). Our algorithm is thus based on the single-

flow-direction approximation (each node has a single receiver) (O'Cal-laghan and Mark, 1984).

The approach we used is based on the work from Braun & Willett (2013) who presented a algorithm to solve very efficiently the stream power equation, regardless of problem geometry or boundary condi-tions. Its main advantages are that the computational time is linearly dependent on the number of nodes used to discretize the landform.

PARALLELIZATION APPROACH

To increase the model's computational efficiency, a two-level mapping parallelism technique is employed.

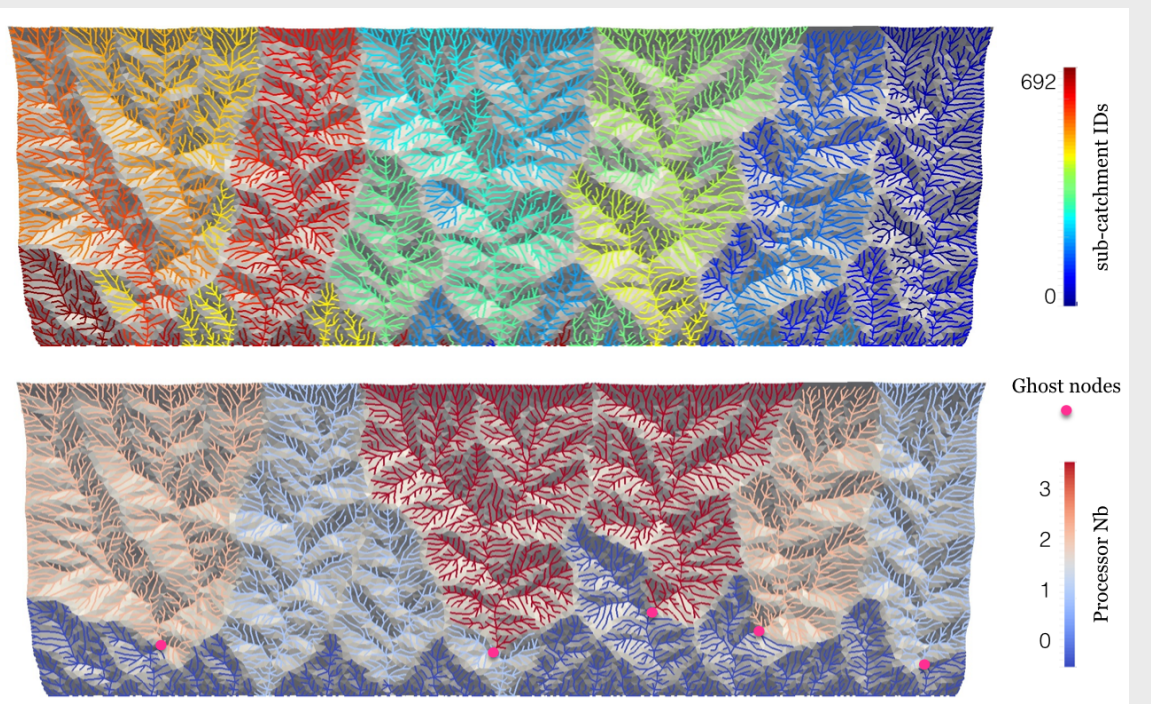
The first level of parallelism handles the mesh partitioning. Features and functions directly related to the mesh and its geometry are re-solved and stored on each partition.

The second level of parallelism is specifically designed to efficiently compute stream network dynamics.

MESH PARTITIONING

At the beginning of a simulation, surface nodes positions representing initial are known. Once the irregular surface has been generated, the set of nodes is partitioned into subdomains. Each subdomain can then be mapped onto a processor of a parallel architecture. For our pur-poses, we consider a mesh partitioner desirable if it produces subdo-mains of nearly equal size (where size is measured by number of nodes) and with as few nodes shared between processors (ghost nodes) as is reasonably possible. The model partitioner uses the Hilbert Space-Filling Curve method algorithm, a description of the method is found in Zoltan library (Catalyurek et al., 2007; Devine et al., 2009).

STREAM NETWORK PARTITIONING



Stream network partitioning strategy. First the drainage is divided in several sub-basins (top figure). Then the partitioning approach consists in (1) minimizing the number of communication points (ghost cells) and (2) splitting the work load (number of nodes) uniformly between processors (bottom figure).

The channel network is used as an acyclic, directed graph, such that reaches and junctions are ordered from upstream to downstream direction. Individual sub-basins draining to channel reaches form the basis for partitioning a large domain into smaller units and synchronizing effort in an upstream to downstream order.

The basic tradeoff in the parallelization of the model is determining how much computational effort occurs in a single sub-basin *vs.* the amount of message passing required between sub-basins. The computational effort in a sub-basin is determined by the number of nodes retained in the TIN and the sub-basin size. Data exchanges between sub-basins consist of lateral surface fluxes through the channel network in upstream to downstream order. Exchanges are performed through message passing using “ghost” cells, which are located at junctions between sub-catchments.

The variables exchanged through ghost cells occur within a model time step according to the sequential order of the processes and the upstream to downstream arrangement of domain nodes. Thus, the computations are synchronized by the structure of the interconnected system of basin nodes. The ghost cells receive, store and send the variables across the TIN nodes when these are located on separate processors.

Sub-basin (or graph) partitioning is generated through the graph partitioning code METIS (Karypis and Kumar, 1999). This approach is based on adjacency in the ordered flow network instead of geographical proximity. The partitioning balances the number of TIN nodes across processors and minimizes the dissections that occur in the channel network through surface ghost cells.

TEMPORAL FRAMEWORK

In **Badlands**, the time evolution of soil thickness and surface elevation is treated explicitly, *i.e.*, the values at the beginning of the next time step are fully determined by the values at the beginning of the ‘current’ time step. The time integration of the continuity equations gives:

$$h_i(t + \Delta t) = h_i(t) + \frac{dh_i}{dt} \Delta t$$

$$z_i(t + \Delta t) = z_i(t) + \left(\frac{dh_i}{dt} - \kappa P_{s,i} + U \right) \Delta t$$

where Δt is the duration of the time steps, and where the values of $P_{s,i}$, U and all time-dependent variables used to calculate dh_i/dt (*i.e.*, the variables involved in the expressions of the soil fluxes) are those at the beginning of the current time step.

Using an explicit time integration scheme, the length of the time steps must be less than a certain time to ensure numerical stability (*i.e.*, to avoid any exponential magnification of approximation errors or numerical artefacts as the simulation proceeds).

CFL-LIKE CONDITIONING

At the beginning of each iteration, the maximal time step is calculated for the adopted first-order, forward-in-time scheme, and is chosen by calculating the minimum CFL factor for the simulated surface processes.

For the simple creep, the CFL factor takes the form:

$$\Delta t_{max} < \min_{ij} \left(\frac{\lambda_{ij}^2}{2\kappa_d} \right)$$

The determination of the CFL limit for the nonlinear diffusion equation is quite tricky (see *e.g.* Pelletier, 2008; Press et al., 1992). We calculate an approximate limit as:

$$\Delta t_{max} \ll \min_{ij} \left(\frac{\lambda_{ij}^2 - \frac{|z_j - z_i|}{S_c^2}}{2\kappa_{nd}} \right)$$

where the inequality is forced by multiplying the right-hand side by a factor such as 0.1 or less. The last expression must be evaluated at each iteration, since it depends on the surface slopes.

For the detachment-limited transport law the CFL upper limit for a given time step is given by:

$$\Delta t_{max} < \min_{ij} \left(\frac{\lambda_{ij}}{\kappa_r q_{w,i}^m \left(\frac{|z_i - z_j|}{\lambda_{ij}} \right)^{n-1}} \right)$$

These CFL conditions serve as initial estimates of required time step but we apply an additional constraint detailed below to ensure numerical stability.

ADJUSTMENT OF SOIL TRANSPORT FLUXES

A straightforward application of the time integration of the continuity equations would lead to incorrect or undesirable results. The main reason is that even with small, though reasonable, time steps, numerical instability may be locally initiated by too-rapid removal or accumulation of soil. To ensure that this undesirable effect never occurs during a simulation, we assume that the amount of soil leaving a cell cannot produce a lowering of surface elevation greater than the difference - multiplied by a factor α (< 1) - of elevation between the cell and its downslope adjacent cell (receiver z_r). And that the amount of deposition inside a given cell cannot be higher than the difference - multiplied by α - of elevation between the cell and the lowest upstream adjacent node z_m . Because diffusive processes tend to smooth out the roughness of the terrain surface, they are not favorable to the initiation of numerical instability. In fact, the addition of a maximum threshold of elevation lowering is only imposed by the action of transport by overland flow. The restrictions described above can be expressed as the following set of inequalities:

$$\begin{aligned} \frac{\Delta t}{\Omega_i} \left(\sum_j w_{ij} q_{s,ij}^{in} - \sum_j w_{ij} q_{s,ij}^{out} \right) &\leq \alpha(z_r - z_i), & \sum_j w_{ij} q_{s,ij}^{out} &> \sum_j w_{ij} q_{s,ij}^{in} \\ &\leq \alpha(z_m - z_i), & \sum_j w_{ij} q_{s,ij}^{in} &> \sum_j w_{ij} q_{s,ij}^{out} \end{aligned}$$

where $q_{s,ij}^{out}$ is the flux of soil leaving the Voronoi cell of the node i , $q_{s,ij}^{in}$ the fluxes of soil coming from the adjacent cells. To meet these restrictions for any amount of available soil and/or soil fluxes of any magnitude, a solution consists in choosing the minimal time step Δt which satisfies this set of inequalities.

REFERENCES

- Braun, J., Sambridge, M., 1997. Modelling landscape evolution on geological time scales: a new method based on irregular spatial discretization. *Basin Research* 9 (1), 27–52.
- Braun, J. and Willett, S.D., 2013. A very efficient, $O(n)$, implicit and parallel method to solve the basic stream power law equation governing fluvial incision and landscape evolution. *Geomorphology*, v.180-181, 170-179.
- Catalyurek, U., E., Boman, K., Devine, D., Bozdag, R., Heaphy, and L., Riesen (2007), Hypergraph-based dynamic load balancing for adaptive scientific computations. IEEE In: Proc. of 21st International Parallel and Distributed Processing Symposium (IPDPS'07).
- Delaunay, B., 1934. Sur la sphère vide. Akademii Nauk SSSR, Otdelenie Matematicheskikh i Estestvennykh Nauk 7, 793–800.
- Devine, K., E., Boman, L., Riesen, U., Catalyurek, and C., Chevalier (2009). Getting started with zoltan: A short tutorial. In: Proceedings of 2009 Dagstuhl Seminar on Combinatorial Scientific Computing.
- Du, C., 1996. An algorithm for automatic Delaunay triangulation of arbitrary planar domains. *Advances in Engineering Software* 27, 21–26.
- Eymard, R., Gallouët, T., Herbin, R., 2000. Finite Volume Methods. In: Ciarlet, P., Lions, J. (Eds.), *Handbook of Numerical Analysis*, Vol. VII. Vol. M. North Holland, Amsterdam, pp. 713–1020.
- Fortune, S., 1992. Voronoi diagrams and Delaunay triangulations. In: Du, D., Hwang, F. (Eds.), *Computing in Euclidian Geometry*. World Scientific, pp. 193–233.
- Gallant, J., Wilson, J., 2000. Primary terrain attributes. In: Wilson, J., Gallant, J. (Eds.), *Terrain Analysis: Principles and Applications*. John Wiley and Sons, New York, pp. 51–85.
- Karypis, G., Kumar, V., 1999. A fast and high quality multilevel scheme for partitioning irregular graphs. *SIAM J. Scientific Comput.* 20 (1), 359–392.
- O’Callaghan, J., Mark, D., 1984. The extraction of drainage networks from digital elevation data. *Computer Vision, Graphics, and Image Processing* 28, 323–344.
- Sambridge, M., Braun, J., McQueen, H., 1995. Geophysical parametrization and interpolation of irregular data using natural neighbours. *Geophysical Journal International* 122 (3), 837–857.
- Tucker, G. E., Lancaster, S. T., Gasparini, N. M., Bras, R. L., Rybarczyk, S. M., 2001a. An object-oriented framework for distributed hydrologic and geomorphic modeling using triangulated irregular networks. *Computers & Geosciences* 27, 959–973.
- Tucker, G. E., Lancaster, S. T., Gasparini, N. M., L, R., 2001b. The channel-hillslope integrated landscape development (CHILD) model. In: Harmon, R. S., Doe, W. (Eds.), *Landscape Erosion and Evolution Modeling*, iii Edition. Kluwer Academic/Plenum, New York, Ch. 12, pp. 349–388.
- Voronoi, G., 1908. Nouvelles applications des paramètres continus à la théorie de formes quadratiques. *Journal für die reine und angewandte Mathematik* 134, 198–287.

SECTION 4

Badlands: installation & dependencies

KEY POINTS

1. Instruction for installation.
2. Dependencies.
3. Compilation.

DEPENDENCIES

This section provides steps and links on obtaining and setting up **Badlands** model. The following instructions assume a beginner's level of familiarity with the Unix/Linux operating environment, including:

- *How to open a terminal window,*
- *How to navigate between directories using a terminal application,*
- *How to open, edit, save and close a file using an editor through a terminal application.*

Badlands relies on a suite of software applications, which need to be installed prior to compiling the code. It is recommended that you install each program in the order listed.

COMPILERS

Badlands is currently supported for GNU compilers , however it works as well with Intel compilers. Both C, C++ and fortran compilers are required.

For Linux OS , they should already been installed with your distribution. GNU compilers for Mac OS can be downloaded from the [HPC](#) website.

To install them you could follow the explanations provided on the website or proceed as follow in a Terminal:

```
$ gunzip gcc-X.X-bin.tar.gz  
$ sudo tar -xvf gcc-X.X-bin.tar -C /
```

It installs everything in `/usr/local`. Then edit your `~/.profile` or `~/.bashrc` and set up the path to the installed compilers.

```
export PATH=/usr/local/bin:$PATH  
export LD_LIBRARY_PATH=/usr/local/lib:$LD_LIBRARY_PATH
```



Now update the configuration file in your Terminal by typing:

```
$ source ~/.profile or ~/.bashrc
```

MESSAGE PASSING INTERFACE

Badlands supports **MPICH** and **OpenMPI**. Below you will find guide to install **MPICH**. **MPICH** can be downloaded from the [here](#). You will need to download the source code such as the **mpich-3.1** (stable release).

Once downloaded, open a Terminal, go to the **untar** folder and do:

```
$ tar -xvf mpich3-xxx.tar  
$ cd mpich3-xxx  
$ CC=gcc FC=gfortran CXX=g++ ./configure --prefix=/usr/local/mpich  
--enable-fast=all --enable-shared --enable-sharedlibs=osx-gcc  
$ make  
$ sudo make install
```

Then edit your **~/.profile** or **~/.bashrc** and set up the path to the installed compilers.

```
export MPI_DIR=/usr/local/mpich  
export PATH=$MPI_DIR/bin:$PATH  
export LD_LIBRARY_PATH= $MPI_DIR/lib:$LD_LIBRARY_PATH
```

Now update the configuration file in your Terminal by typing:

```
$ source ~/.profile or ~/.bashrc
```

HDF5

HDF5 can be downloaded from the [Hdf5](#) website. You will need to download the source code available for all platform such as the **HDF5-1.8.13** release. Once downloaded, open a Terminal and navigate to the **untar** folder and do:

```
$ CC=mpicc FC=mpif90 ./configure --prefix=/usr/local/hdf5 --enable-parallel --enable-fortran
```

After the configuration script has finished, checked the summary of the log which is printed on your screen and ensure that both **HDF5** for Fortran and C are present as well as the **HDF5** compression facility (**zlib**). If **zlib** is missing you will have to install it first following documentation in the [zlib](#) website.

```
$ make  
$ sudo make install
```

XML PARSER

FoX XmL can be downloaded from [there](#). You will need to download the source code available as a tarball such as **FoX=4.1.2.tar.gz**. Once downloaded, open a Terminal and navigate to the **untar** folder and do:

```
$ cd FoX-xxx  
$ FCFLAGS='-O2 -fPIC' FC=mpif90 ./configure --prefix=/usr/local/FoX  
$ make  
$ sudo make install
```

Once compiled, you will need to open the **/usr/local/FoX/bin/FoX-config** file using your preferred editing file:

```
$ sudo emacs /usr/local/FoX/bin/FoX-config
```

And change the **comp_prefix** (third line of the file) to the correct prefix in this case: **/usr/local/FoX** and delete the **/objs** at the end of the path.

METIS

The **Metis** library is available from [there](#). Once downloaded, open a Terminal and navigate to the **untar** folder and do:

```
$ cd metis-xxx
```

```
$ make config cc=mpicc prefix=/usr/local/metis  
$ sudo make install
```

ZOLTAN

Zoltan needs to be downloaded from Sandia [website](#). Once downloaded, open a Terminal and create a building folder:

```
$ mkdir zoltanbuild  
$ cd zoltanbuild  
$ ../Zoltan_v3.81/configure --enable-f90interface --enable-mpi --with-  
mpi-compilers --with-gnumake --prefix=/usr/local/zoltan  
$ make everything  
$ sudo make install
```

ESMF

ESMF can be obtained from [here](#). Once downloaded **untar** folder and in the terminal set the following paths:

```
$ export CC=/usr/local/bin/gcc  
$ export CXX=/usr/local/bin/g++  
$ export FC=/usr/local/bin/gfortran  
$ export CPP=/usr/local/bin/cpp
```

Then edit your **~/.profile** or **~/.bashrc** and set up the following path:

```
export ESMF_DIR=/usr/local/esmf  
export ESMF_BOPT=O  
export ESMF_OPTLEVEL=3  
export ESMF_COMM=mpich2  
export ESMF_COMPILER=gfortran  
export ESMF_ABI=64  
export ESMF_OS=Darwin  
export ESMF_LAPACK="internal"
```

```
export ESMF_XERCES=  
export ESMF_NETCDF=  
export ESMF_PNETCDF=  
export ESMF PIO=  
export ESMF_INSTALL_PREFIX=/usr/local/esmfinstall  
export ESMF_INSTALL_MODDIR=$ESMF_INSTALL_PREFIX/mod  
export ESMF_INSTALL_LIBDIR=$ESMF_INSTALL_PREFIX/lib  
export ESMF_INSTALL_HEADERDIR=$ESMF_INSTALL_PREFIX/header  
export ESMF_INSTALL_BINDIR=$ESMF_INSTALL_PREFIX/bin  
export ESMFMKFILE=$ESMF_INSTALL_LIBDIR/esmf.mk
```

Now update the configuration file in your Terminal by typing:

```
$ source ~/.profile or ~/.bashrc
```

Then in the Terminal do:

```
$ make  
$ make install
```

FIRE-UP BADLANDS

Badlands can be cloned from GitHub.

```
$ git clone git://github.com/badlands-model/Badlands.git
```

Please always refer to the above site for latest software updates. Prior to starting the compilation process, you will need to check the path to the libraries you've installed on your system as they might differ from one to the other. In Badlands, the configuration are set in the **config** folder. The folder contains several files associated to different environments *e.g.* Linux/Mac or Intel/Gnu. Depending on the ones you've installed, copy the corresponding file and edit it:

```
$ cp Makefile.cfg.osx Makefile.cfg.myconfig  
$ emacs Makefile.cfg.myconfig
```

In the file, check that the paths are set correctly. If not sure look at your `~/.profile` or `~/.bashrc`. Make the necessary changes and save your file. Now open the **Makefile.inc** file and change the first line to match with your new configuration file name:

```
CFGFILE = $(TOP)/config/Makefile.cfg.myconfig
```

Then compile Badlands sources from the top directory:

```
$ make clobber  
$ make dist
```



SECTION 5

Badlands: input files

KEY POINTS

1. General parameters.
2. Forcing parameters.
3. Processes parameters.

Badlands is using **XML** input file. **XML** language, compared to standard **ASCII**, is well formatted and has a controlled structure. The **XML** input file has both constraints on the structure and content of the elements which are used to control the parameters of the simulation.

External **ASCII** files (formatted in **csv**) are referenced inside the **XML** document and provide information on the basal node position, the changes in forcing parameters, *e.g.* uplift/subsidence, rainfall and sea level. To start with a working **XML** input file it is recommended to use one of the examples provided in the next chapter.

GENERAL PARAMETERS

GEOMETRY

The first structure which appears in the input file is related to the definition of the geometry: initial surface (regular grid) & triangular irregular network (**TIN**) parametrization.

`<regular_grid>`

refers to the name of the regular surface nodes file **ASCII** and its path. The path is from the main input file location. The file provides for each line the following information:

- X coordinates in meters (this axis has a West to East orientation),
- Y coordinates in meters (this axis has a South to North orientation), &
- Z coordinates in meters.

Nodes must be defined in increasing order from the South/North corner, first along the X axis.

`<delaunay_area>`

sets a maximum area constraint when generating the Delaunay triangulation. No triangle will be generated whose area is larger than that number. This area should be at least equal to a regular grid cell area.

<delaunay_angle>

sets a minimum angle constraint when generating the Delaunay triangulation. If the minimum angle is 20.7° or smaller, the triangulation algorithm is theoretically guaranteed to terminate. In practice, the algorithm often succeeds for minimum angles up to 33° . It usually doesn't terminate for angles above 34° .

<refine_area>

defines the number of high resolution areas in the simulation.

<ra>

initial entry class to set the properties of a specific high resolution area. A high resolution area is defined as a squared box which extends have to be defined within the simulated area and be at least two regular grid cells inside the domain. If the refine_area is set to 0 this **XML** component is not required.

- <xmin> SW X corner of the considered high resolution area,
- <ymin> SW Y corner of the considered high resolution area,
- <xmax> NE X corner of the considered high resolution area,
- <ymax> NE Y corner of the considered high resolution area,
- <r_area> set high resolution area.

Setting up the boundary conditions on the simulation domain:

- <boundN> Northern boundary condition,
- <boundS> Southern boundary condition,
- <boundE> Eastern boundary condition,
- <boundW> Western boundary condition.

Possible values for these fields are 0,1,2. Where 0 defines a fixed boundary, 1 a wall and 2 a slope boundary. By default the value is set to 2 for all borders.

- <outlet> defines an outlet on one of the corner of simulation area (allowed values are: 1 for SW corner, 2 for SE corner, 3 for NW corner and 4 for NE corner). When defining an outlet the previous boundary conditions will be set to 1 (wall boundary).

<output_directory>

Name of the output folder where both simulation results and run files will be stored. The directory is divided in two sub-directories:

- one called **outputs** which record simulation output,
- one called **runfiles** which record simulation informations

Note: the outputs sub-directory contains time-series files that can be visualized in **Paraview** or **Visit**.

Note: the **runfiles** sub-directory contains the checkpointing files required to restart a simulation.

Note: to preserve previous runs, you will have to change the output directory name otherwise it will be automatically rewritten and previous outputs will be lost.

TIME

The second structure defines simulation and processes time steps.

- <time_start> starting time of the simulation,
- <time_end> ending time of the simulation,
- <display_interval> time interval to create output.

In addition and if we are restarting a previous simulation:

- <restart_folder> name of the previous simulation folder,
- <restart_fileID> time interval of the restarted simulation,
- <restart_petNb> number of processors used in previous run,
- <time_step> set time step for the run (deprecated),
- <limit_step> flag (0 or 1), value of 1 precludes the use of adapting time step, default is 0.

FORCING PARAMETERS

SEA-LEVEL FLUCTUATIONS

Optional structure which define ocean fluctuations.

<**ocean_file**> name of the **csv** file containing the sea level evolution through time. This **ASCII** file provides for each line the following information:

- time in years,
- sea-level elevation for the considered time in meters.

In addition the defined fluctuation times should be set in increasing order starting from the oldest time.

UPLIFT/SUBSIDENCE EVOLUTION

Optional structure which define tectonic displacements.

- <**interval_nb**> total number of displacement intervals that will be simulated. The displacement intervals need to be declared by increasing time and should not overlap with each others,
- <**disp**> definition of an individual displacement field,
- <**disp_start**> time in years at which the considered vertical displacement will start,
- <**disp_end**> Time in years at which the considered vertical displacement will end,
- <**disp_file**> name of the displacement file and its associated path.
The path is from the main input file location.

The displacement **ASCII** file provides at each line the cumulative vertical displacement for each considered node in meters.

Attention: the file defines the cumulative displacement during the duration defined above and not a displacement rate.

Note: the nodes are read in increasing order based on the regular grid discretization starting from the South-West corner and going first along the X axis (West to East).

UNDERWORLD COUPLING

Instead of using the previous Uplift/subsidence definition it is possible to use the soft coupling between Underworld model and Badlands.

To work the plugin requires that both Underworld and Badlands have been compiled on the same machine. In Underworld specific input parameters have to be turn on to enable the coupling.

The communications between the codes are done at specific time steps and are driven by a file called 'maestro' localized in a synchronization folder known by each code.

Badlands will provide to Underworld is a **vtk** file containing top surface information ('**topsurface.vtk**').

Underworld will provide to Badlands an **ASCII** file containing vertical displacement fields ('**uw_output.ascii**').

Note: the plugin only looks at vertical displacements.

- <**sync_folder**> path to the synchronization folder used by each code to read and write required coupling files. The path is from the main input file location,
- <**sync_time**> time step for synchronization.

CLIMATE EVOLUTION

To simulate overland flows it is essential to defines rainfall parameters and regime. It is possible to specify a series of maps files with rainfall values defined for each nodes.

<**rain_nb**> defines the number of rainfall series imported for the considered simulation.

<rain> collection of rainfall parameters defining each series.

Note: the number of classes needs to be equal to the number given in the **<rain_nb>** element.

- **<rain_start>** start time of the considered rainfall grid interval in years,
- **<rain_end>** end time of the considered rainfall grid interval in years,
- **<rain_file>** name of the rainfall file and its associated path. The path is from the main input file location.

This **ASCII** file provides for at each line the averaged precipitation in meters/year.

Note: the nodes need to be defined in increasing order based on the regular grid discretization starting from the South-West corner and going first along the X axis (West to East)

Note: in case a specific node does not have any precipitation it is required to set it in the file with a 0.0 value.

OVERLAND FLOW PARAMETERS

DETACHMENT LIMITED

Model equation:

$$\mathbf{q}_r = -\kappa_r (q_w)^m (\nabla z)^n$$

For detachment limited transport (stream power law), the following parameters are required.

<spl_m> corresponds to the coefficient m in the equation.

<spl_n> corresponds to the coefficient n in the equation.

<Cerodibility> corresponds to the coefficient κ_r in the equation.

In case where you are interested in purely erosive system the optional element below could be set to increase the computational time:

<pureErosion> to take into account erosion only, possible values are 0 or 1.

UNDER-CAPACITY MODEL

Model equations:

$$\begin{aligned}\mathbf{q}_e &= -\kappa_f S A \\ \frac{\partial h}{\partial t} &= \left(\frac{q_r - q_e}{\omega_c L_b} \right) \text{ if } h \leq h_0 \\ \frac{\partial h}{\partial t} &= \left(\frac{q_r - q_e}{\omega_c L_a} \right) \text{ if } h > h_0\end{aligned}$$

For under-capacity transport, the following parameters are required.

<bedrock_length> length scale characterizing the erodibility of bedrock L_b .

<alluvial_length> length scale characterizing the erodibility of alluvial L_a .

<stream_erosion> corresponds to the coefficient κ_f in the equation.

<bedrock_sediment_interface> initial thickness of regolith depth.

<channel_exp> channel width exponent α_c .

<channel_width> channel width coefficient β_c .

REGOLITH PRODUCTION

Model equation:

$$P_s = P_0 e^{-h/h_0}$$

Regolith production is defined by:

<rego_prod> corresponds to parameter P_0 in the equation.

<rego_depth> corresponds to parameter h_0 in the equation.

<soil_density> density of soil ρ_s .

<rock_density> density of bedrock ρ_r .

<diff_m> corresponds to the coefficient p in the equation.

<diff_n> corresponds to the coefficient l in the equation.

<coef_depthdepend_aerial> κ_{dd} in aerial environment.

<coef_depthdepend_marine> κ_{dd} in marine environment.

Hillslope parameters

SIMPLE CREEP

Model equation:

$$\mathbf{q}_d = -\kappa_d \nabla z$$

For simple creep, the following parameters are required:

<coef_linear_aerial> κ_d parameter in aerial environment.

<coef_linear_marine> κ_d parameter in marine environment.

NON-LINEAR DIFFUSION

Model equation:

$$\mathbf{q}_{nd} = -\frac{\kappa_{nd} \nabla z}{1 - \left(\frac{|\nabla z|}{S_c}\right)^2}$$

For non-linear diffusion,

<coef_non_linear_aerial> κ_{nd} in aerial environment.

<coef_non_linear_marine> κ_{nd} in marine environment.

<slope_critical> critical slope S_c .

DEPTH-DEPENDENT DIFFUSION

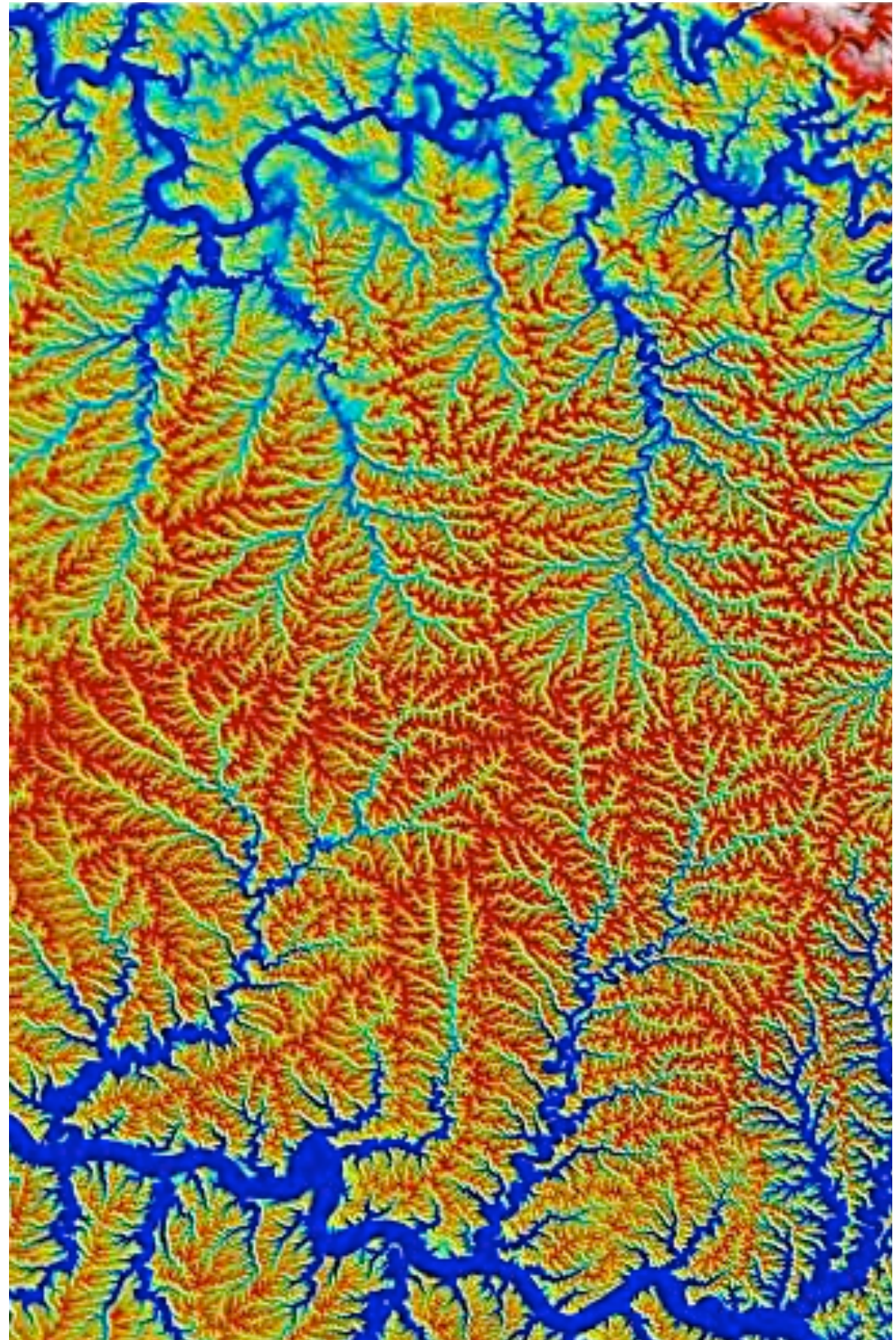
Model equation:

$$\mathbf{q}_{dd} = -\kappa_{dd} h^p (\nabla z)^l$$

For depth-dependent diffusion:

Badlands model: Applications

All tests provided in the following section are available from GitHub:
<http://github.com/badlands-model/Badlands-doc.git>



SECTION 1

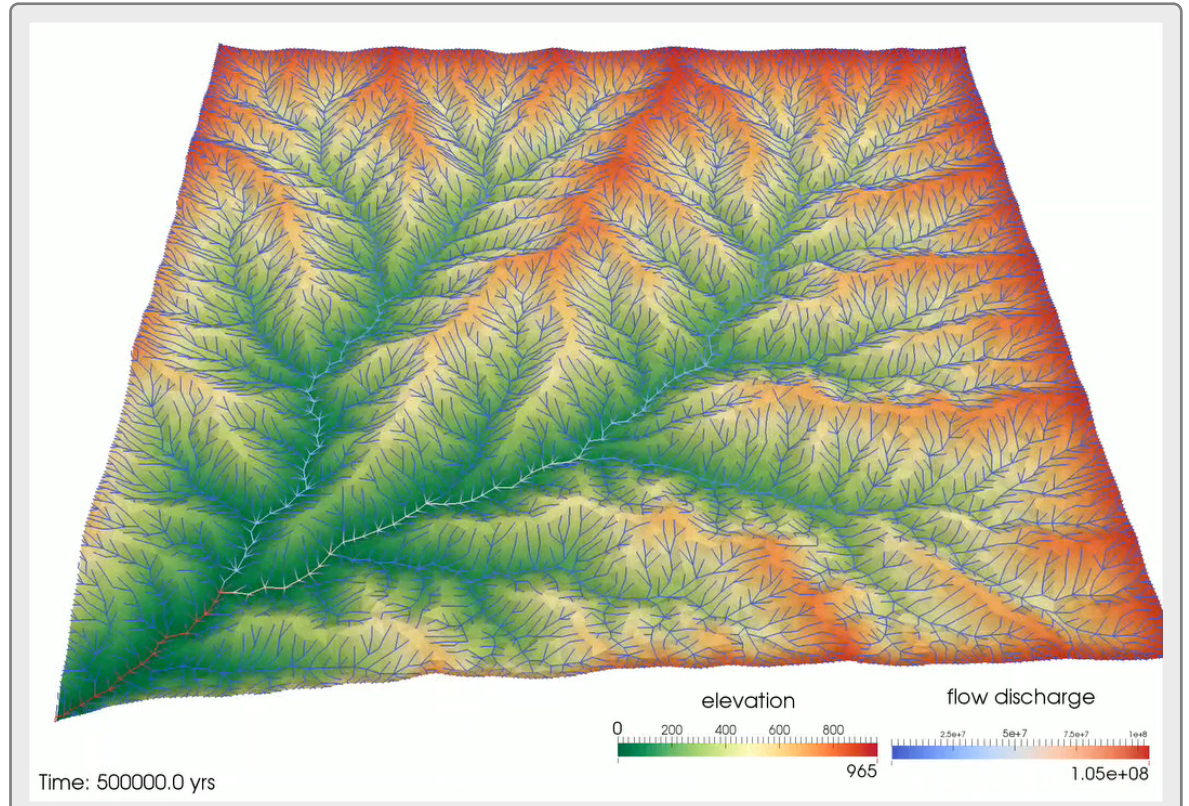
Planar surface with single outlet

KEY POINTS

1. Experimental settings.
2. River profile.
3. Sensitivity analysis
4. Under-capacity model

PLANAR SURFACE WITH SINGLE OUTLET

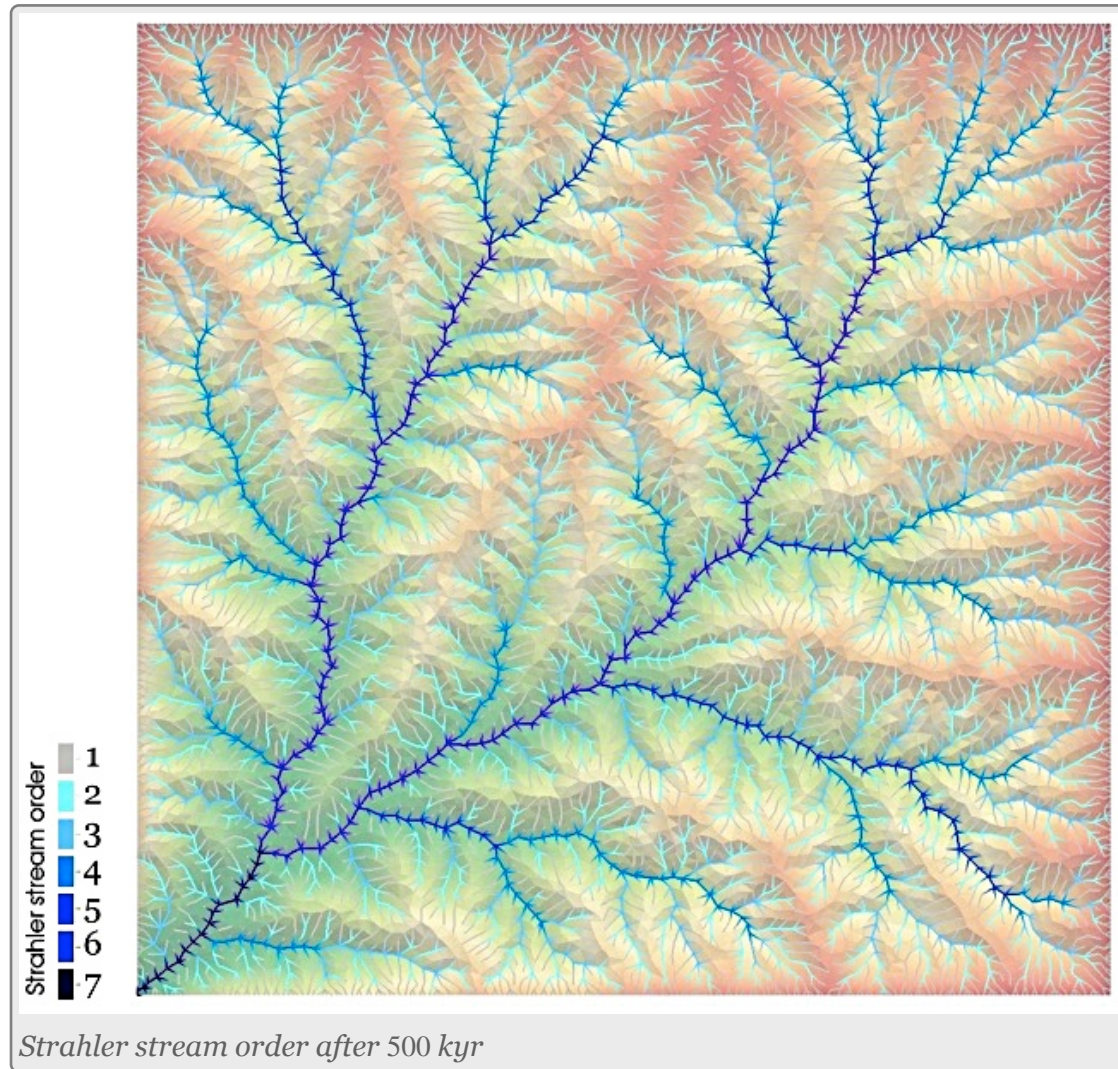
INITIAL CONDITIONS



Surface evolution of a horizontal plane with a single outlet subject to uniform uplift and rainfall.

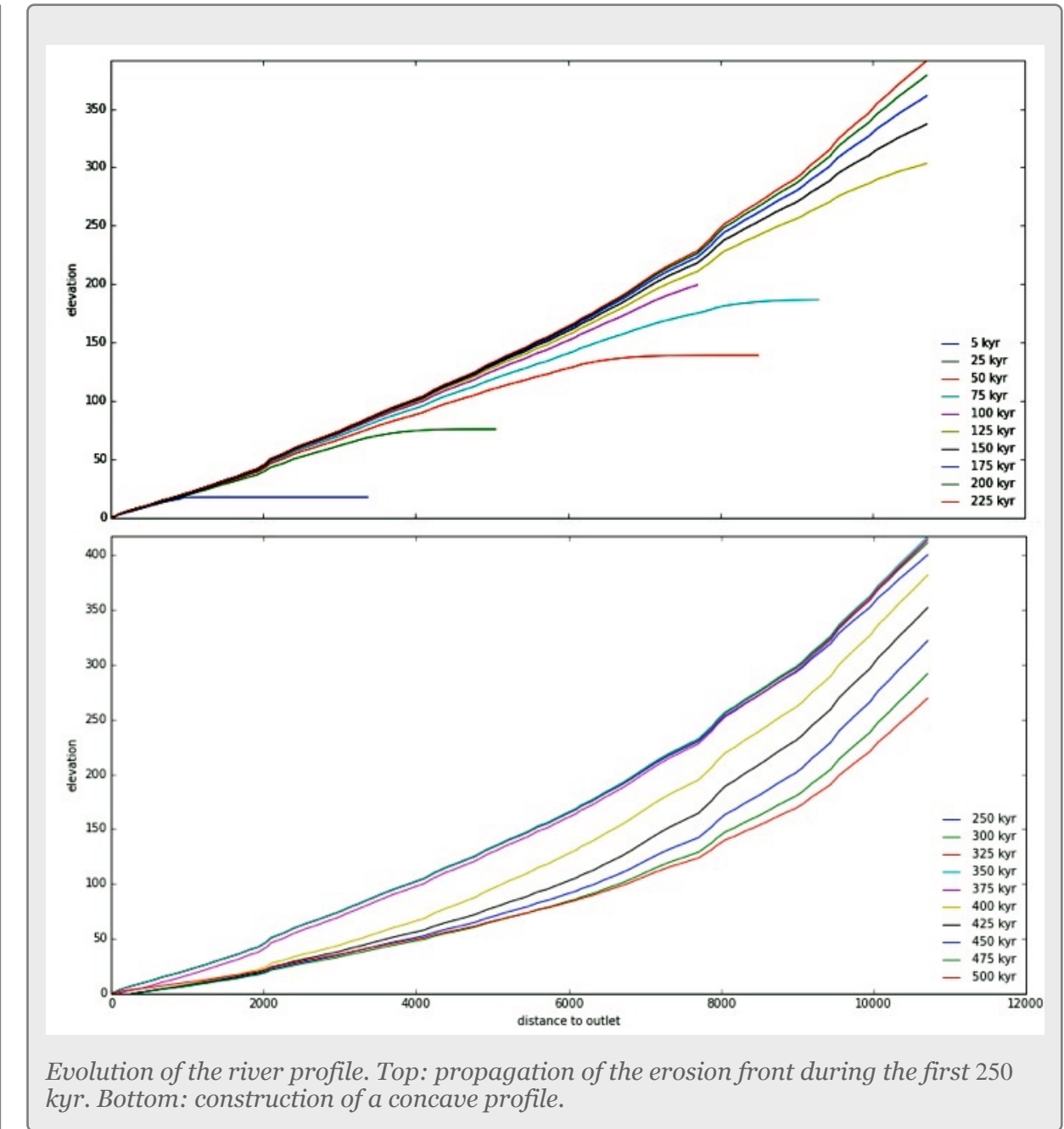
Above animation shows an example of surface simulation starting from a horizontal topographic surface of size $10 \times 10 \text{ km}^2$, sampled randomly on about 10,000 points, that evolves through a time span of 500 kyr. The uplift rate is set to 1 mm/yr everywhere except on the outlet point where a subsidence of 0.2 mm/yr is imposed. The rainfall is set to 1 m/yr over the entire domain. All surface boundary points are closed, except for a single open outlet at (0,0) coordinates. This surface is allowed to evolve by simulating linear diffusion (*simple creep*) and detachment limited overland flow processes. Diffusion is implemented with a uniform diffusivity constant $\kappa_d = 0.1 \text{ m}^2/\text{yr}$. Erosion due to channeling is simulated with the following parameters: $\kappa_r = 10^{-5} \text{ m}^{1-2m}/\text{yr}$; $m = 0.5$; $n = 1$. Note that, in this simulation, all the model parameters are con-

stant and uniform. The only spatially random element is given here by the position of the sampled points. A developed drainage network is already visible after 50 kyr evolution, as a result of competition between diffusive hillslope transport and channel incision processes. After 250 kyr, the surface has evolved and forms a fully developed, dendritic drainage pattern with maximum stream order of 7 over the last portion of the catchment just before reaching the outlet. Over the last 200 kyr the drainage pattern is stabilized.

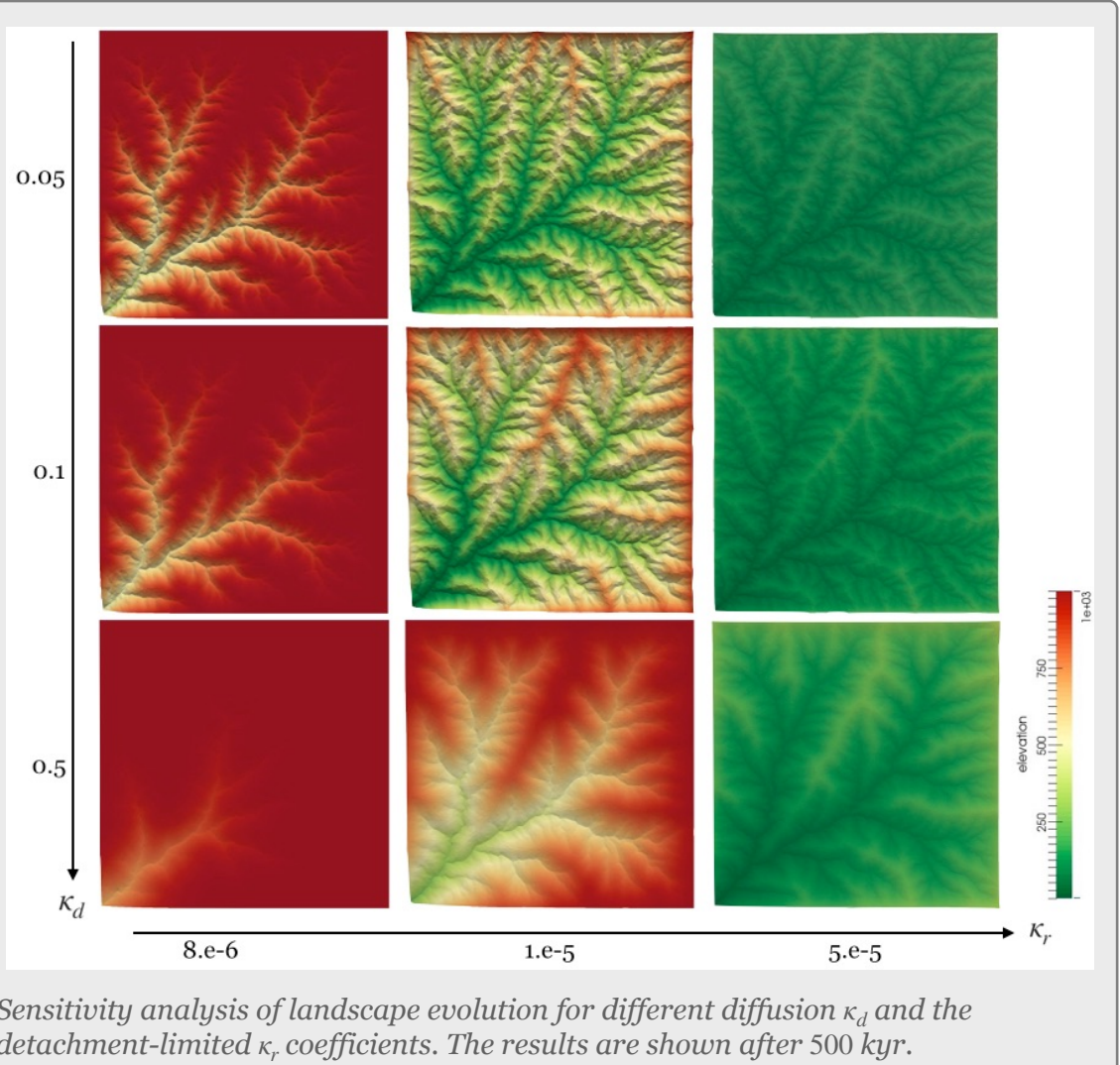


RIVER PROFILE EVOLUTION

To underline more quantitatively the consistency of the simulation, it is possible to represent a series of profiles of one particular river (the

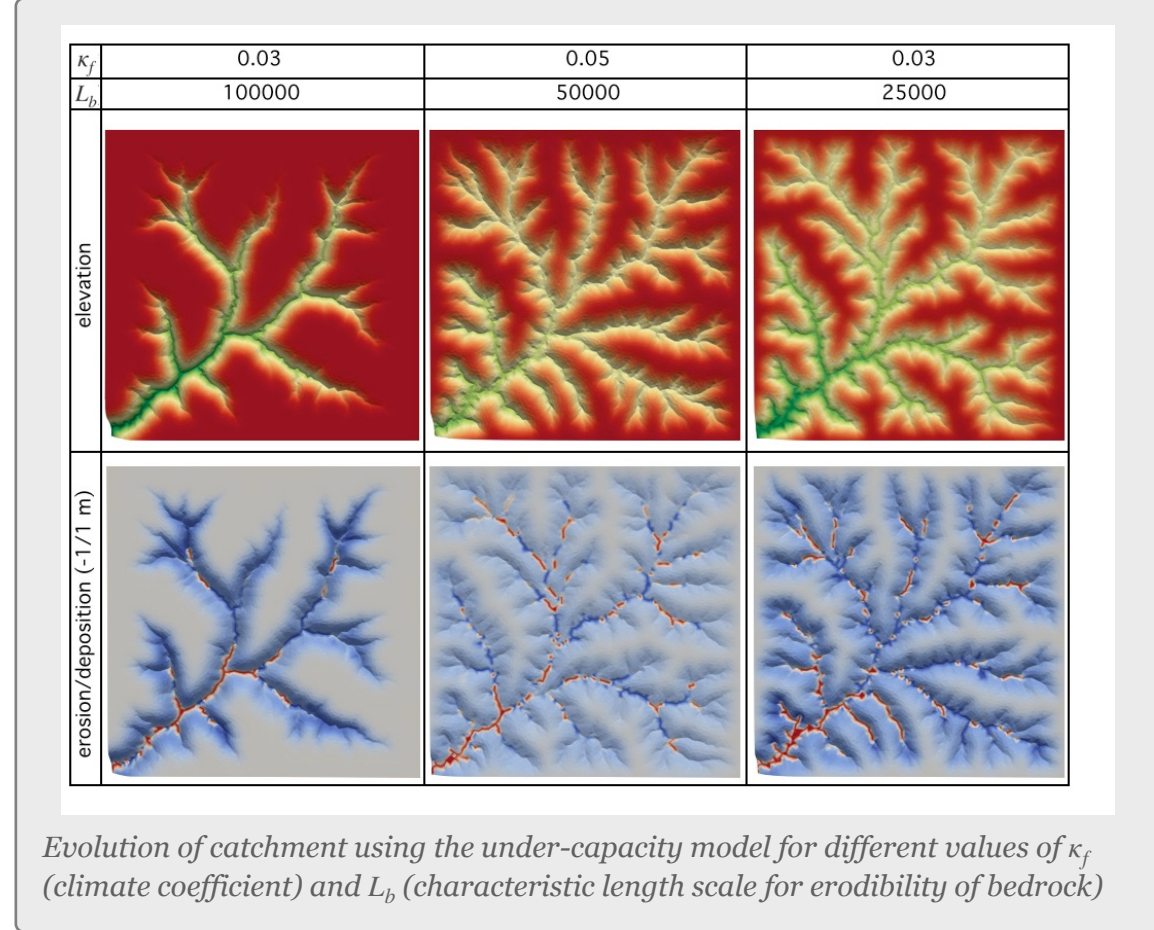


longest visible blue line roughly on the bottom diagonal of the squared domain) extracted from the TIN surface. We observe the progression of erosion in the upslope direction as time passes (top figure), indicated symbolically by the grey arrow. By a simulated time of 200 kyr, the entire river course has settled and the river profile shows an upward concavity (bottom figure).



SENSITIVITY ANALYSIS

Model sensitivity to both diffusion and detachment limited coefficient is explored for 3 different values of κ_d and κ_r . The results presented in the next figure shows how the landscape has evolved for a considered period of 500 kyr. We observe that increase in hillslope processes magnitude (increase in κ_d) leads to a “smoothing” of surface topography but does not produce changes in the final morphology of the river network. The effect of κ_r is tested by varying it between $8.10^{-6} - 5.10^{-5}$. Because it is a constant of proportionality, varying κ_r influences the rate of landscape evolution; if κ_r is increased by more than 10 for the considered set of model parameter, the landscape erodes nearly instantaneously.



UNDER-CAPACITY MODEL

The under-capacity model is a sediment flux dependent model where the detachment rate depends on degree to which sediment flux falls below transport capacity. Therefore even if the considered model is mainly erosive, it shows, unlike the previous detachment-limited tests, areas of deposition within the valleys (colored in red in the bottom figures). The diffusion parameter κ_d for all these tests is equal to 0.1.

FURTHER READING

Refice, A. Giachetta, E., Capolongo, D. (2012). SIGNUM: a Matlab, TIN-based landscape evolution model, Computers & Geosciences 45, 293-303.

Castelltort, S. Yamato, P. (2013). The influence of surface slope on the shape of river basins: Comparison between nature and numerical landscape simulations, Geomorphology 192, 71–79.

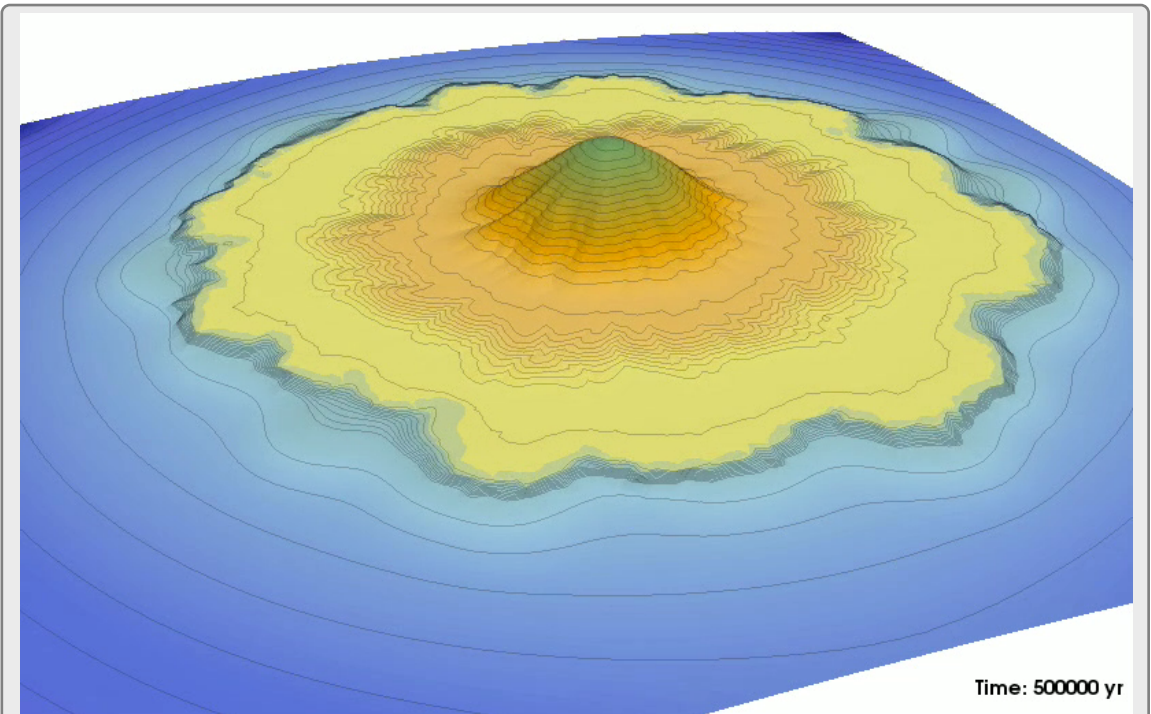
SECTION 2

Delta evolution & sea-level fluctuations

KEY POINTS

1. Experimental settings.
2. Hillslope & overland flow models.
3. Depositional/erosional patterns.
4. Stratigraphic evolution.

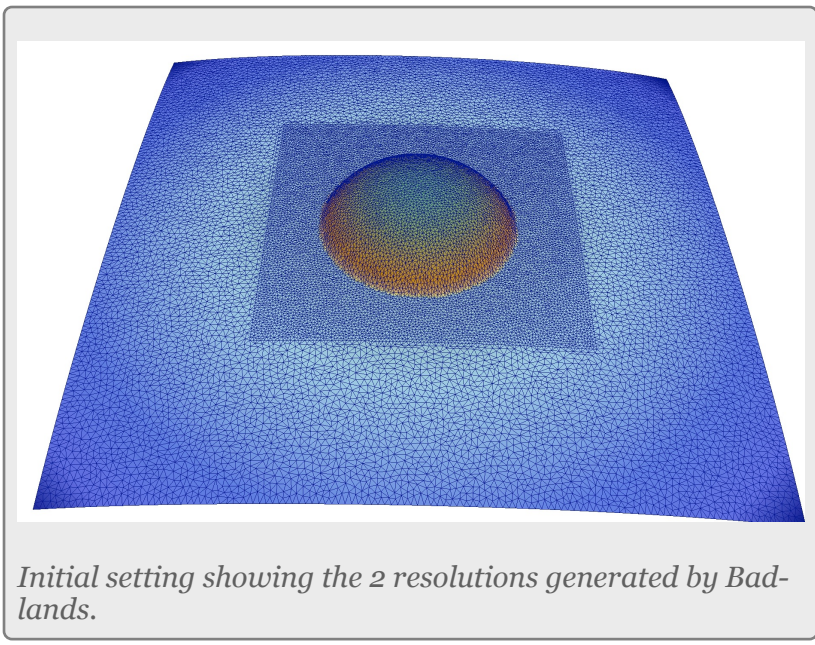
SEDIMENT TRANSFER, DELTA FORMATION AND SEA-LEVEL VARIATION



Mountainous landscape evolution with sedimentation front evolving over time subject to sea-level fluctuations.

EXPERIMENTAL SETTINGS

The initial surface defines a mount which is a half ellipsoid of 2000 m height and about 8 km large. The sea-level is initially set at the base of this mount at a elevation of 0 m. An uniform precipitation rate of 1 m/yr is applied on the all area and we test the evolution of the surface due to both hillslopes and overland flows. Two hillslope coefficient are defined for both the aerial and marine area. The simulation runs for 500,000 years and we vary the sea-level through time (values are defined in table next page). From its initial setting, we first perform a sea-level drop of 100 m after 200,000 years than we come back to the initial sea level at 300,000 years. We then perform a second cycle, this time by imposing a sea-level rise of 100 m for around 100,000 years, then finally, we reset the sea-level to 0 m until the end of the simulation.



TIME	SEA LEVEL
0	0
180,000	0
200,000	-100
280,000	-100
300,000	0
320,000	100
380,000	100
400,000	0
500,000	0

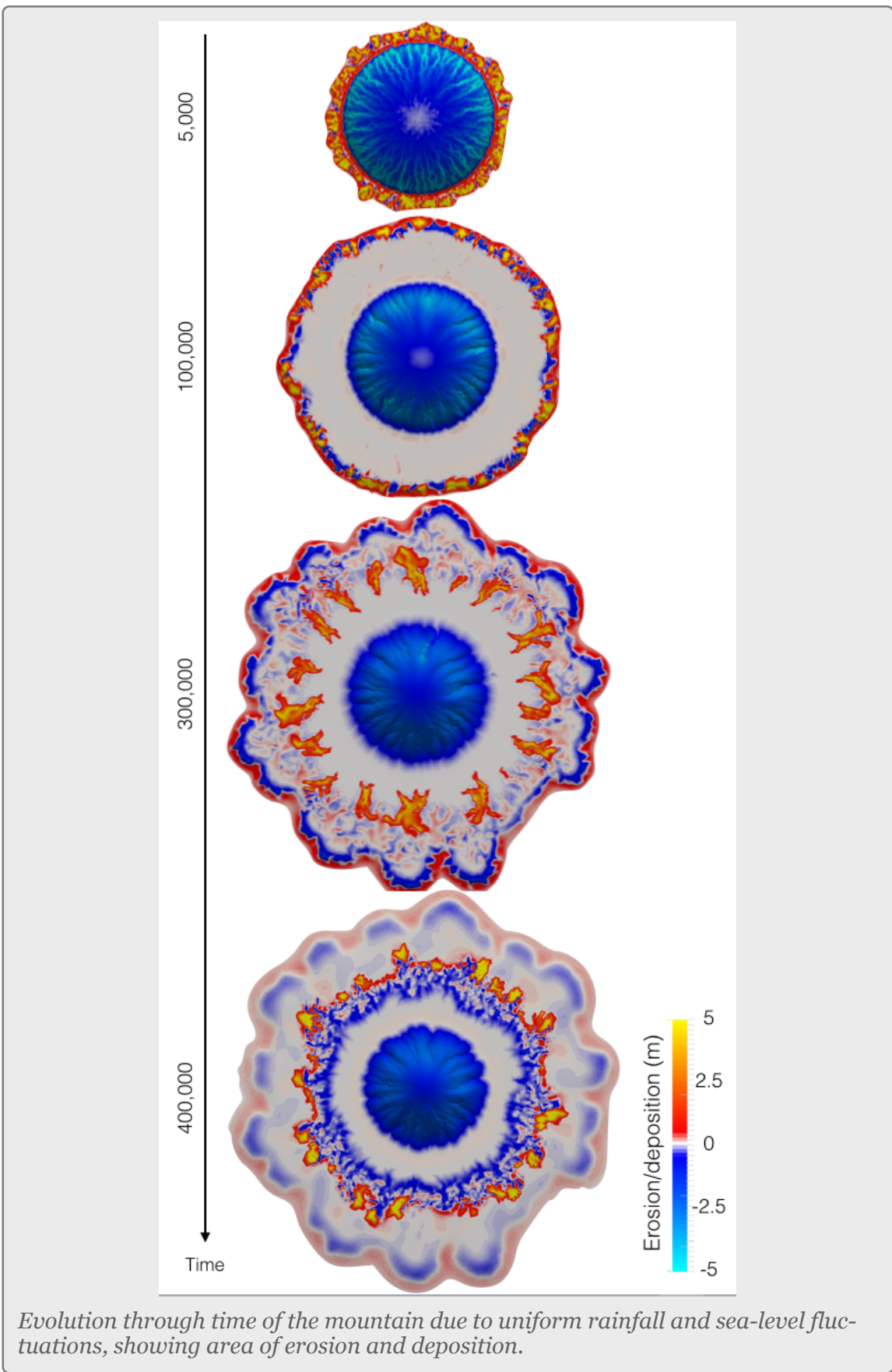
In addition, the grid is divided in two resolutions by defining a bounding box within the input file. A high-resolution area ($10,000\text{ m}^2$) is chosen around the mount, whereas the marine environment has a lower resolution of $40,000\text{ m}^2$.

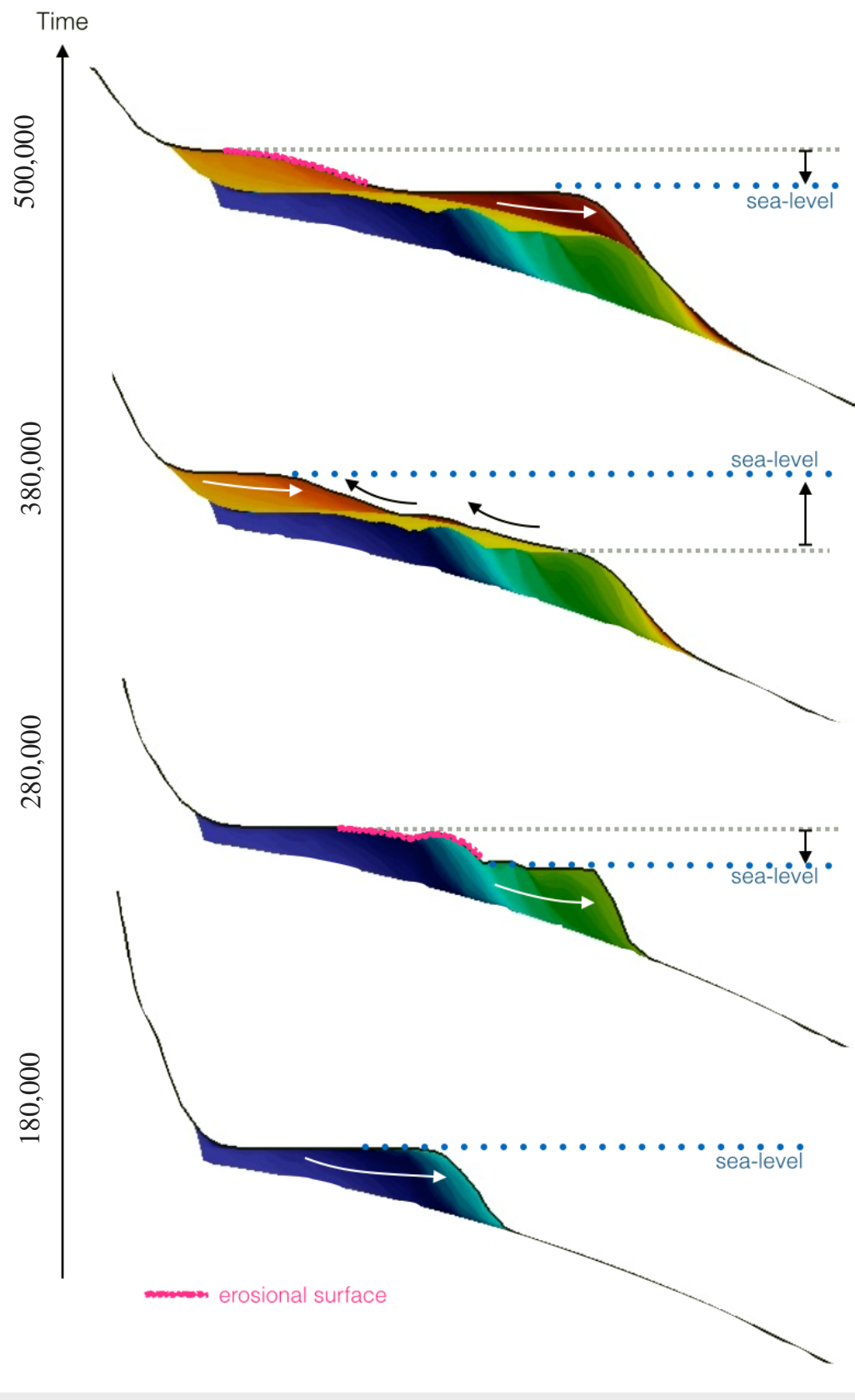
DEPOSITIONAL/EROSIONAL PATTERNS & SEQUENCE STRATIGRAPHY

During the first phase of the simulation the mount is eroded and sediment are transported in the marine environment where we see a sedimentation front prograding towards the marine environment (two top views in the next figure).

As the sea-level falls, it creates a condition of forced regression, in which the coast is forced to build seaward. During the falling stage, rivers begin to incise on what was formerly a marine shelf, forming incised valleys. These incised valleys tend to widen and grow landwards. From 200,000 – 280,000 years, the low-stand system marks the greatest extent of subaerial exposure and erosion.

As the rate of relative sea-level rise increases, it leads to retrogradational parasequence stacking also refers as transgressive systems. Dur-

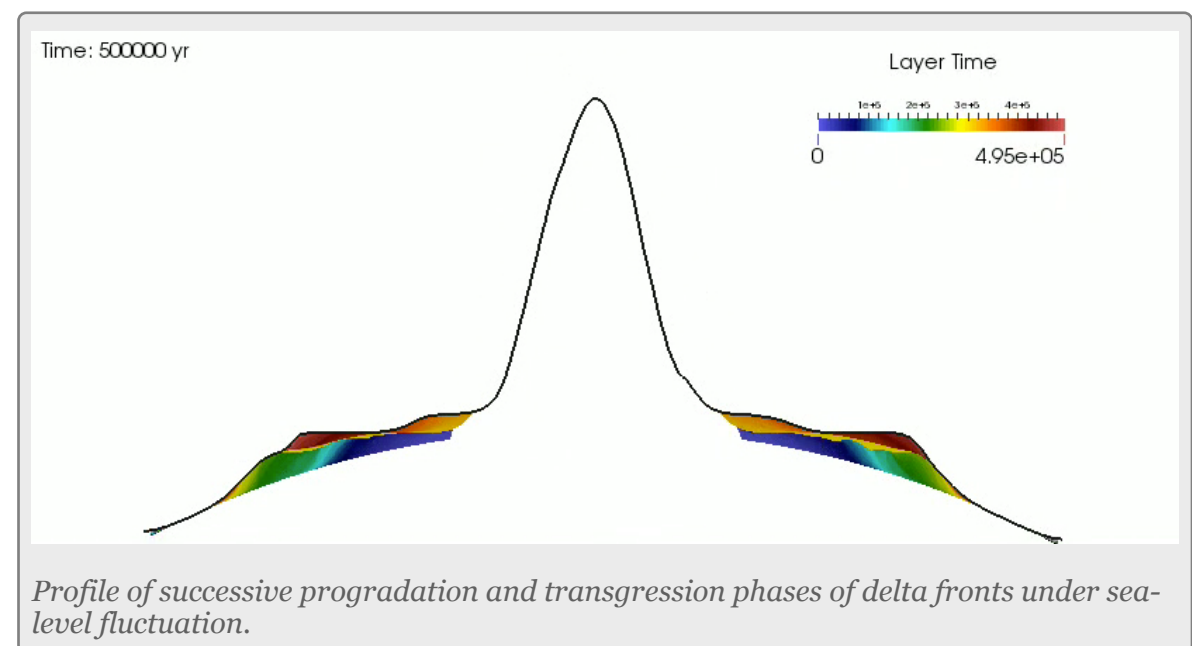




ing this stage the the previously incised valleys are filled as shown in the previous figure at 300,000 years.

Between 320,000 – 380,000 yrs, the sedimentary system turns from retrogradational stacking in the transgressive system to progradational stacking in the highstand system. During this stage, the sediment supply to the shelf favors the development of progradational sequences.

During the last 100,000 years, the system returns to its original sea-level which is mark by incision of formerly marine shelf deposits and development of a new sedimentation front.



FURTHER READING

Coe, A. L., 2002. The Sedimentary Record of Sea-Level Change. Cambridge, New York: Cambridge University Press. pp. 57–98

Hampson, G.J., Davies, S. J., Elliott, T., Flint, S. S., Stollhofen, H., 1999. Incised valley fill sandstone bodies in Upper Carboniferous fluvio-deltaic strata: recognition and reservoir characterisation of Southern North Sea analogues. In: Petroleum Geology of NW Europe: Proceedings of the 5th Conference. (Edited by Fleet, A.J. & Boldy, S.A.R.). The Geological Society, London. 771-788.

Catuneanu, O., 2003. Sequence stratigraphy of clastic systems. St. John's Nfld.: Geological Association of Canada

SECTION 3

Climatic forcing on drainage evolution

KEY POINTS

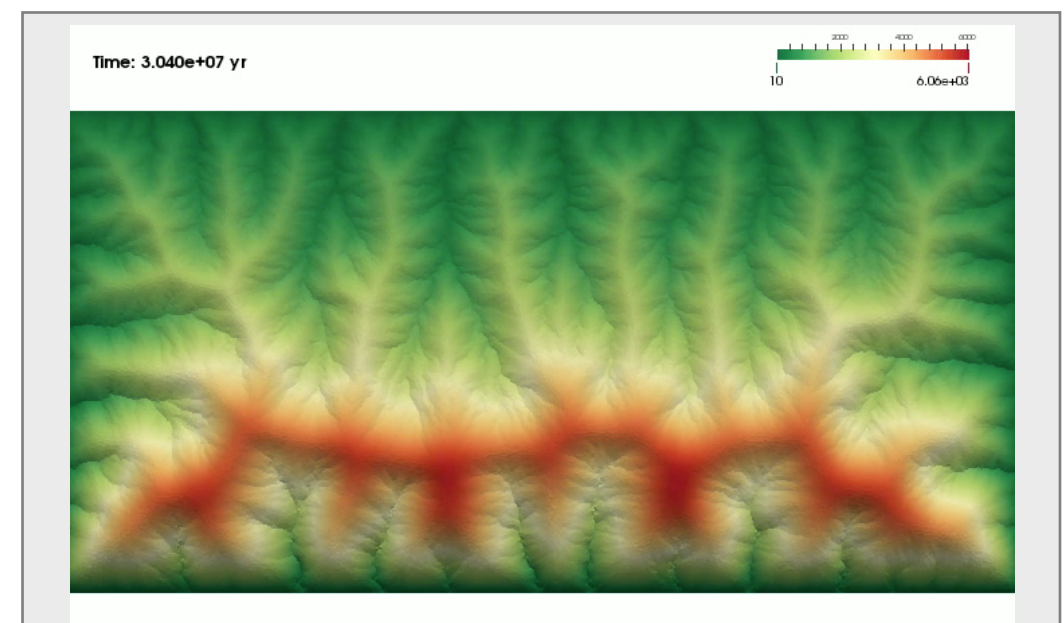
1. Experimental settings.
2. Natural analogues.
3. Temporal evolution of catchments.

ROLE OF CLIMATE CHANGE IN DRAINAGE NETWORK REORGANIZATION

The continuous feedbacks among tectonics, surface processes, and climate change are reflected in the distribution of catchments on active mountain fronts.

Previous studies have shown a certain regularity of valley spacing on several mountain ranges worldwide, but what is at the origin of such geomorphological feature of landscapes is currently not well known.

This example illustrate long-term landscape evolution of an active mountain range. It shows how the constant valley spacing, achieved at steady state on both sides of the range, is progressively restored after simulating a migration of the main drainage divide caused by a precipitation gradient applied across the mountain belt.



From an initial steady state, drainage network reorganization under an imposed precipitation gradient.

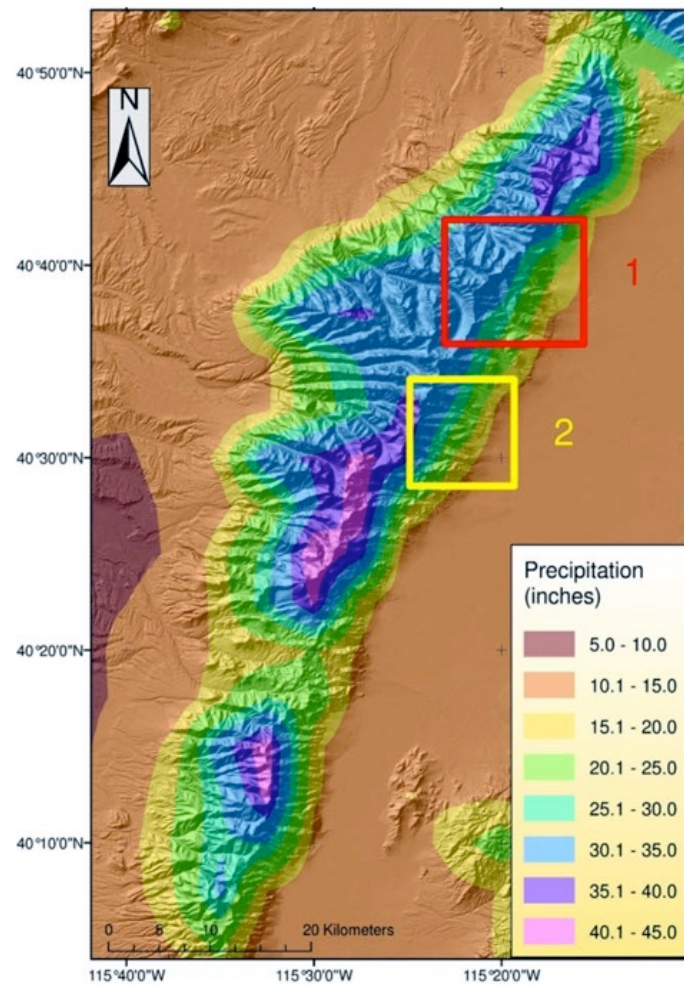
EXPERIMENTAL SETTINGS

We simulate landscapes of various sizes, with a fixed TIN mean sampling distance of 100 m; the initial surface is completely flat at zero ele-

vation. Sediment can flow across all four landscape boundaries. We apply a spatially uniform and constant uplift rate of 1 mm/yr over the whole domain.

After the initial topography has reached a steady state under a uniform, constant precipitation rate of 1 m/yr, a precipitation gradient is introduced, in a direction perpendicular to the belt axis, to simulate "orographic" precipitation; the maximum precipitation rate is set to 3 m/yr along the upper side, and it linearly decreases towards the opposite side reaching a minimum of 0.1 m/yr.

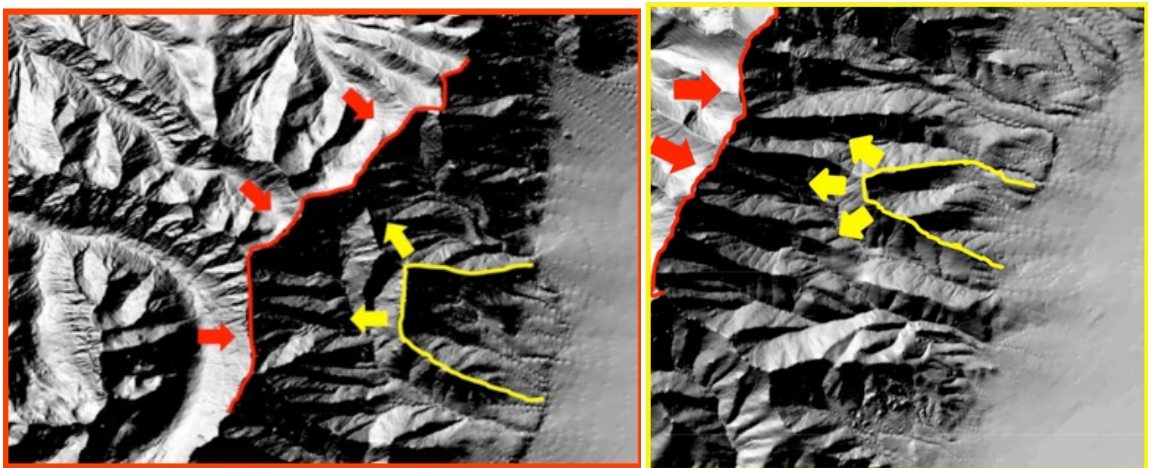
NATURAL EXAMPLES



A real-world example of the behavior corresponding to the simulated numerical results described above can be seen along the Ruby Mountains, as suggested by Ellis et al. (1999).

In the Basin and Range area, the air circulation is mainly from West to East. When moist air from the Pacific Ocean encounters a topographic barrier such as the Ruby Mountains, it is forced to move upward and over the obstacle, losing moisture in form of heavy precipitation on the western flank. This also results in a lack of precipitation on the eastern side of the range.

A PRISM (Daly et al., 1994) average annual precipitation map of the area from the period 1961-1990 is shown in the top figure. The Ruby Mountains are an uplifted core complex, bounded by active normal faults and there are enough similarities to warrant comparison with our numerical modeling results.

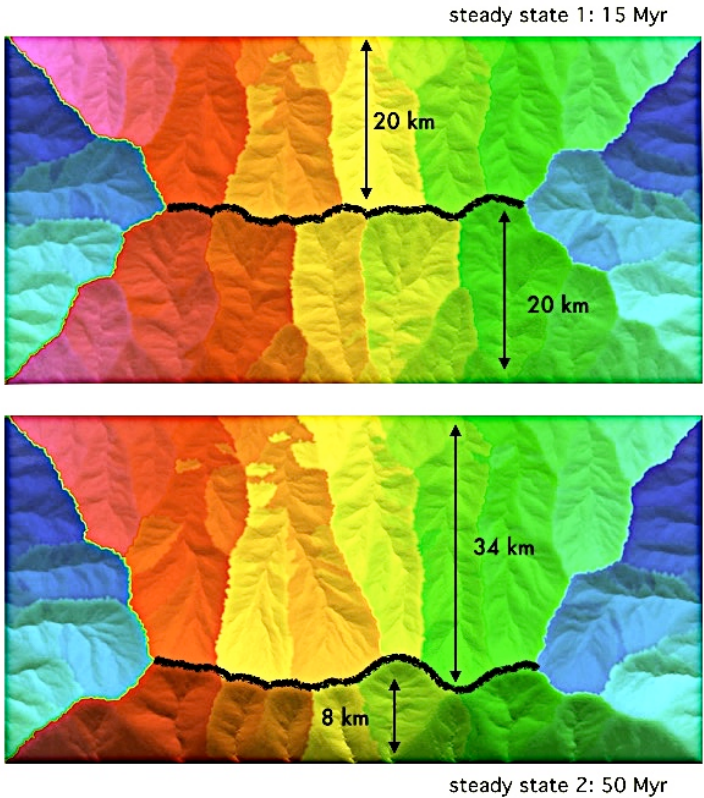


We know that the drainage basins emphasized here have been significantly impacted by geomorphic processes neglected in the numerical model (glaciation and cirque headwall processes that accompany alpine glaciations). In fact, the rivers that currently drain the Ruby Mountains are largely out of equilibrium with respect to their long profiles and sediment transport, because they have inherited valleys significantly modified by recent glaciations.

Nevertheless, some analogies between the transient topography in the numerical model simulation and on the leeward side of the Ruby range are highlighted in bottom figures. In particular, potential examples of the main drainage divide migration, the shrinking of the larger catchments and the growth of triangular facets, which look similar to the simulated basins in our numerical experiments, are highlighted.

TEMPORAL EVOLUTION OF RIVER CATCHMENTS

The landscape reached the first steady-state topography under uniform precipitation after 15 Myr. The pattern of catchments, illustrated in the top right figure, consists of an alternation of larger, and smaller catch-



Top: landscape has reached the steady-state topography under uniform precipitation. Bottom: development of the second steady-state topography under a precipitation gradient. Middle line shows the drainage divide for both states.

network and maximum stream order is consequently reduced in the larger watersheds.

A new steady state topography is reached under changed climatic conditions. The numerical results show that change in the precipitation pattern exerts a strong control on drainage network development and reorganization on both sides of the simulated mountain belt. In particular, the leeward side shows a more interesting evolution, where the interaction amongst all geomorphic processes leads to a significant catchment reorganization.

The final result of this complex mechanism of watershed reorganization is a new steady state topography.

ments etched on the triangular facets. The catchments on the North and South side of the mean drainage divide exhibit the same elongated characteristics.

After the precipitation gradient is applied, the main divide of the belt is pushed from the wet side (northern part) towards the dry side (southern part), where larger catchments shrink and, simultaneously, the smaller catchments on triangular facets grow. Furthermore, the drainage

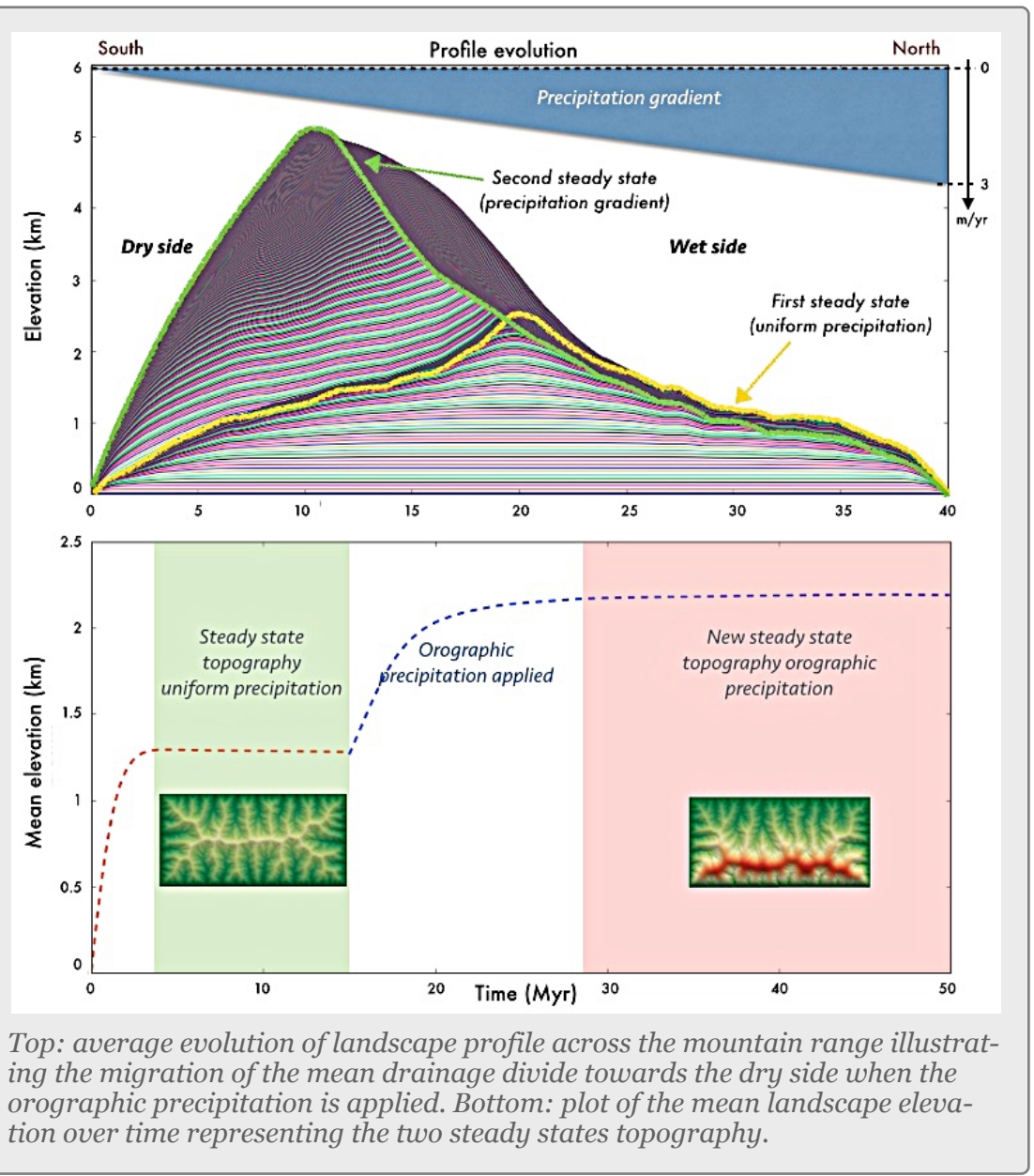
Furthermore, the model of watersheds development proposed here, can explain some real landscapes in which we found analogies with the different evolutionary stages of the simulated belts.



Drainage network evolution for a considered catchment after imposing the precipitation gradient.

REFERENCES

- Bonnet, S. (2009). Shrinking and splitting of drainage basins in orogenic landscapes from the migration of the main drainage divide, *Nature Geoscience*, 2:11, p. 766-771.
- Daly, C., Neilson, R.P., and Phillips, D.L. (1994). A statistical-topographic model for mapping climatological precipitation over mountainous terrain. *Journal of Applied Meteorology*, v. 33, 140–158.
- Ellis, M., Densmore, A.L., and Anderson, R.S. (1999). Development of mountainous topography in the Basin Ranges, USA, *Basin Research*, v. 11, p. 21–41.
- Hovius, N. (1996), Regular spacing of drainage outlets from linear mountain belts, *Basin Research*, 8, 29-44. Perron, J.T., Kirchner, J.W., and Dietrich, W.E. (2009). Formation of evenly spaced ridges and valleys, *Nature* 460, 502-505.
- PRISM Climate Group (2006), Oregon State University: <http://prism.oregonstate.edu>.
- Refice, A., Giachetta, E., Capolongo, D. (2012). SIGNUM: a Matlab, TIN-based landscape evolution model, *Computers & Geosciences*. 45, p. 293-303.



Tucker, G.E., Lancaster, S.T., Gasparini, N.M., Bras, R.L. and Rybarczyk, S.M. (2001). An Object-oriented Framework for Distributed Hydrologic and Geomorphic Modeling using Triangulated Irregular Networks. *Computers & Geosciences*. 27: 959-973.

Wallace, R.E. (1978). Geometry and rate of changes of fault-generated range fronts, northcentral Nevada. *Jour. Research U.S. Geol. Survey*, 6, 637-650.

SECTION 4

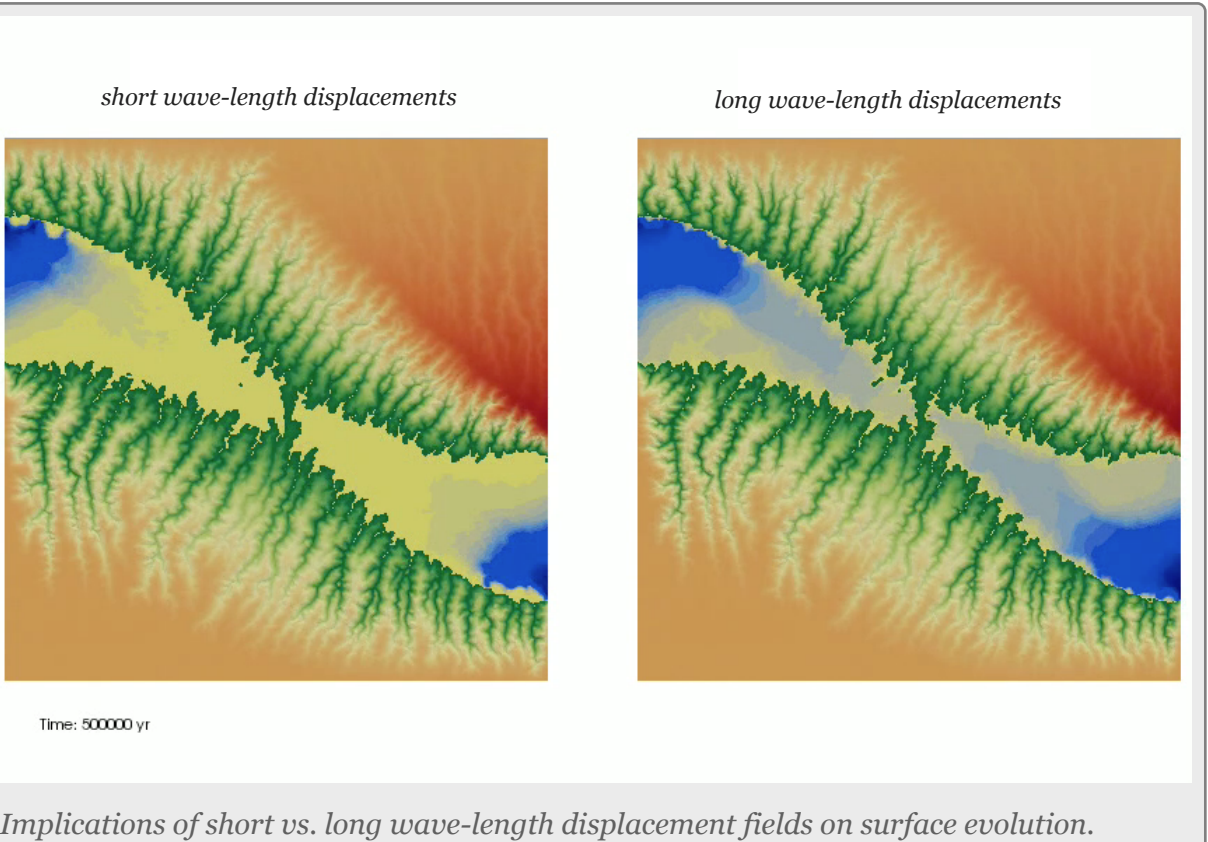
Tectonic forcing and basin evolution

KEY POINTS

1. Experimental settings.
2. Displacement fields.
3. Stratigraphic evolution.

IMPOSED RIFTING DISPLACEMENTS

Interlinks between deformation and sedimentation have long been recognized as an important factor in the evolution of continental rifts and basins development. However, determining the relative impact of tectonic and climatic forcing on the dynamics of these systems remains a major challenge.

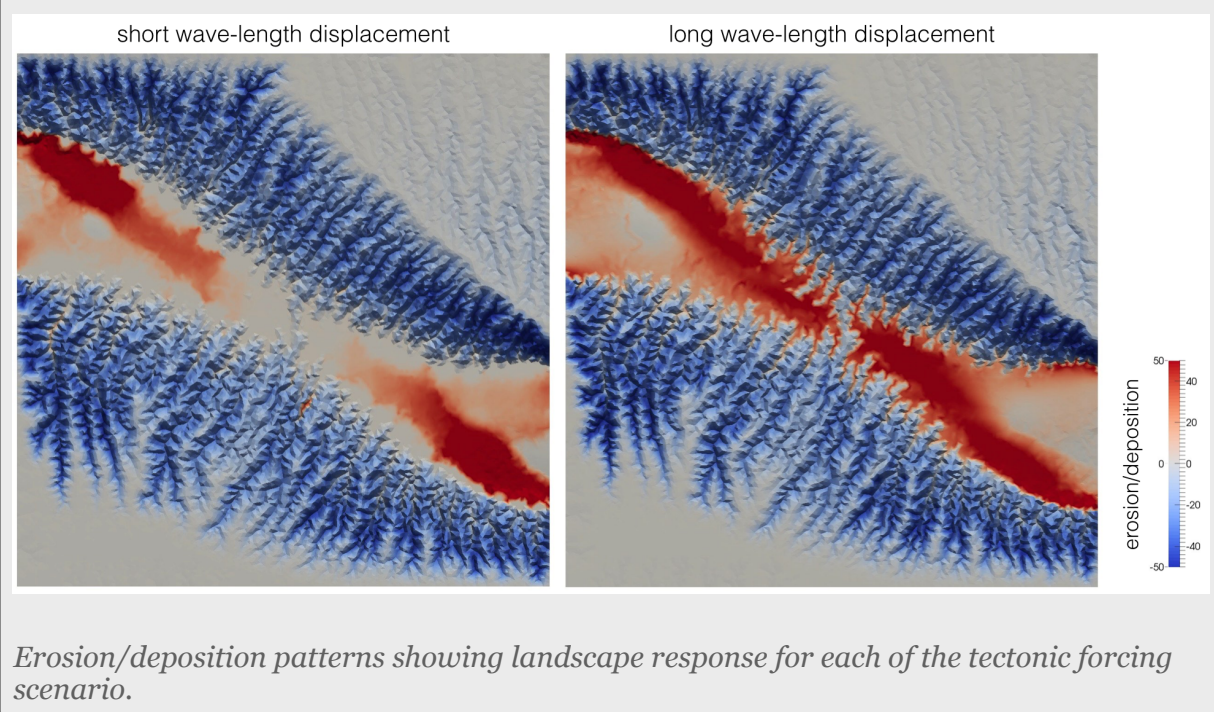


EXPERIMENTAL SETTINGS

In this example, we impose over 500,000 years a 3D oblique rifting displacement field produced with *Underworld* over an initial flat surface. We consider both hillslope (creep) and overland flow processes (detachment limited) induced by an uniform precipitation rate of 1 m/yr.

The displacement field obtained from *Underworld* gives us an average rate of uplift/subsidence over a time frame of several thousand years. Here, we test with Badlands the effects of *short wave-length/high am-*

plitude versus *long wave-length/low amplitude* displacements on geomorphologic evolution and basin sedimentation.



DISPLACEMENT FIELDS

For the first experiment, we apply rapid displacement rate of high amplitude in short time scales (between 1 to 10 years). These pulses create a rapid disequilibrium of the landscape morphology which is balanced by high and localized rates of erosion and sedimentation.

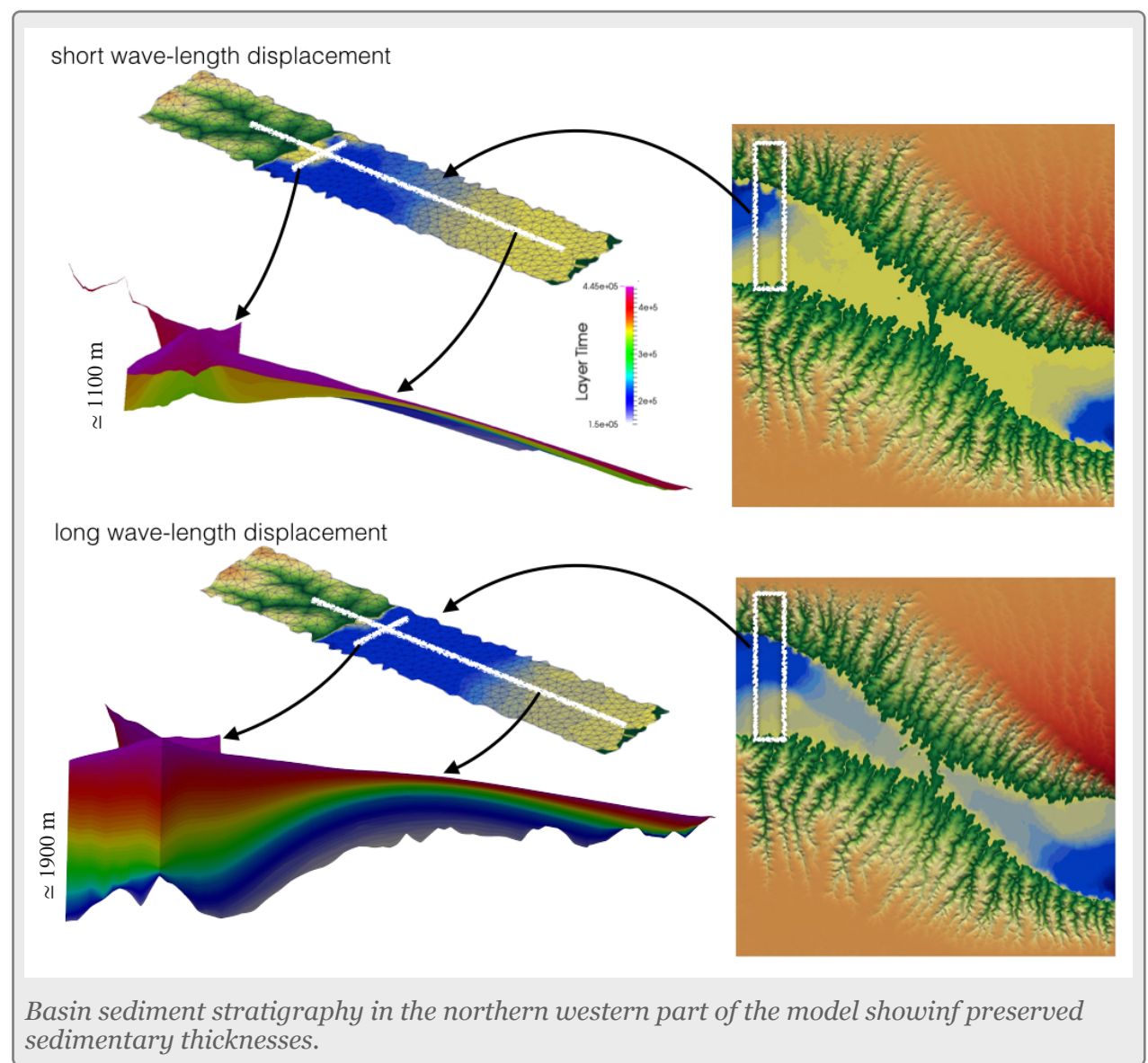
For the second experiment, the displacements are uniformly distributed over time with the same amplitude as for experiment one but applied on time scales ranging from 20,000 to 100,000 years. Hillslope and overland flow processes, in this case, attenuate the tectonic perturbations over time.

At the end of the simulation after 500,000 years, the two resulting topographies show similar erosional patterns on both side of the rifting zone. The obtained valleys have similar shapes, directions and heights. In the central part of the rifted system, which is mainly depositional, the geo-

morphology appears to be different. For the first experiment the marine intrusion is more pronounced with development of several deltaic systems at the mouth of distributary valleys during periods of high tectonic rates.

STRATIGRAPHIC EVOLUTION

Recorded basin stratigraphy (bottom figure) shows the difference in thickness of preserved sediments for the 2 cases. For the second experiment, most of the sedimentary history is preserved within the sequence from 150,000 up to 500,000 years with a cumulative thickness reaches



nearly 2000 m in the deepest part of the basin. The first case shows a different response with a much thinner preserved sedimentary thickness (\approx 1100 m) and a series of hiatus and unconformities through the sequence.

REFERENCES

Hilley, G. E., and Arrowsmith J R. (2008). Geomorphic response to uplift along the Dragon's Back pressure ridge, Carrizo Plain, California, *Geology*, v. 36; no. 5; p. 367–370; doi: 10.1130/G24517A.1, 2008.

Hurst, M. D., Mudd, S. M., Attal, M., and Hilley G. (2013). Hillslopes record the growth and decay of landscapes, *Science*, 23 2013: 341 (6148), 868-871.

Luke, M., Duclaux, G., Salles, T., Thomas, C., Rey, P. (2013). Stratigraphic Modelling of Continental Rifting, EGU - Austria, id. EGU2013-6616